Article

Cell

Crystal Structure of Silkworm PIWI-Clade Argonaute Siwi Bound to piRNA

Graphical Abstract

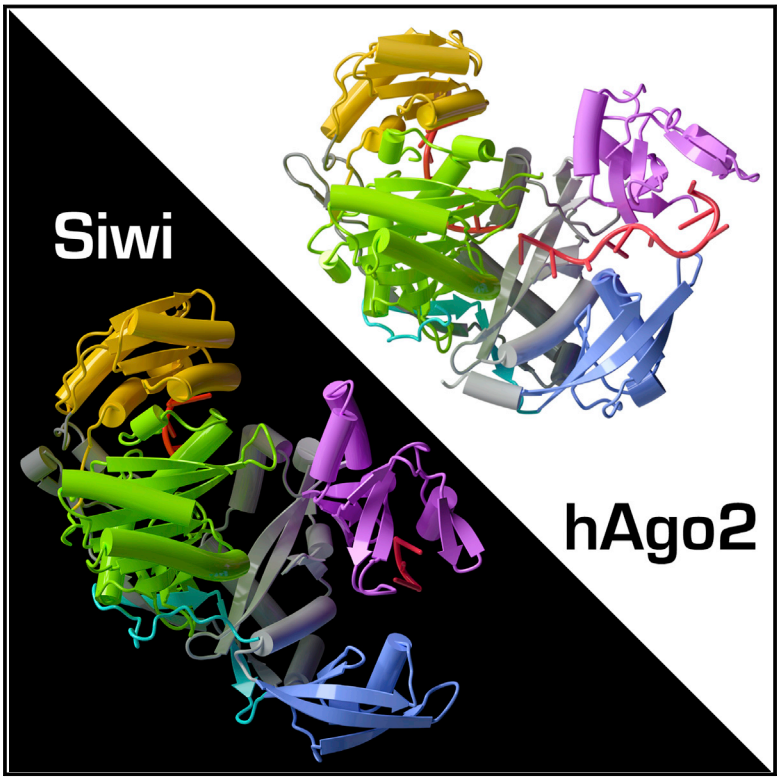

Authors

Naoki Matsumoto, Hiroshi Nishimasu, Kazuhiro Sakakibara, ..., Haruhiko Siomi, Mikiko C. Siomi, Osamu Nureki

Correspondence

nisimasu@bs.s.u-tokyo.ac.jp (H.N.), siomim@bs.s.u-tokyo.ac.jp (M.C.S.), nureki@bs.s.u-tokyo.ac.jp (O.N.)

In Brief

The first structure of the PIWI protein reveals mechanistic insights into its target recognition and cleavage.

Highlights

- Crystal structure of a PIWI-clade Argonaute bound to piRNA
- Structural basis for the preference of Siwi for the guide 1U
- Specific recognition mechanism of the 5′ and 3′ ends of the bound piRNA by Siwi
- Structural similarities and differences between AGO- and PIWI-clade Argonautes

Data Resources

5GUH

Matsumoto et al., 2016, Cell *167*, 484–497
October 6, 2016
http://dx.doi.org/10.1016/j.cell.2016.09.002

CellPress

Cell

Article

Crystal Structure of Silkworm PIWI-Clade Argonaute Siwi Bound to piRNA

Naoki Matsumoto,[1,4] Hiroshi Nishimasu,[1,2,4,*] Kazuhiro Sakakibara,[1] Kazumichi M. Nishida,[1] Takamasa Hirano,[3] Ryuichiro Ishitani,[1] Haruhiko Siomi,[3] Mikiko C. Siomi,[1,*] and Osamu Nureki[1,5,*]

[1]Graduate School of Science, Department of Biological Sciences, The University of Tokyo, 2-11-16 Yayoi, Bunkyo-ku, Tokyo 113-0032, Japan

[2]JST, PRESTO, 2-11-16 Yayoi, Bunkyo-ku, Tokyo 113-0032, Japan

[3]Keio University School of Medicine, 35 Shinanomachi, Shinjuku-ku, Tokyo 160-8582, Japan

[4]Co-first author

[5]Lead Contact

*Correspondence: nisimasu@bs.s.u-tokyo.ac.jp (H.N.), siomim@bs.s.u-tokyo.ac.jp (M.C.S.), nureki@bs.s.u-tokyo.ac.jp (O.N.)

http://dx.doi.org/10.1016/j.cell.2016.09.002

SUMMARY

PIWI-clade Argonaute proteins associate with PIWI-interacting RNAs (piRNAs) and silence transposable elements in animal gonads. Here, we report the crystal structure of a silkworm PIWI-clade Argonaute, Siwi, bound to the endogenous piRNA, at 2.4 Å resolution. Siwi adopts a bilobed architecture consisting of N-PAZ and MID-PIWI lobes, in which the 5′ and 3′ ends of the bound piRNA are anchored by the MID-PIWI and PAZ domains, respectively. A structural comparison of Siwi with AGO-clade Argonautes reveals notable differences in their nucleic-acid-binding channels, likely reflecting the distinct lengths of their guide RNAs and their mechanistic differences in guide RNA loading and cleavage product release. In addition, the structure reveals that Siwi and prokaryotic, but not eukaryotic, AGO-clade Argonautes share unexpected similarities, such as metal-dependent 5′-phosphate recognition and a potential structural transition during the catalytic-tetrad formation. Overall, this study provides a critical starting point toward a mechanistic understanding of piRNA-mediated transposon silencing.

INTRODUCTION

Argonaute proteins associate with small RNA guides and form RNA-induced silencing complexes (RISCs), which repress target RNAs complementary to the guide RNAs at the transcriptional or posttranscriptional level (Siomi and Siomi, 2009; Ghildiyal and Zamore, 2009; Czech and Hannon, 2011; Meister, 2013). The Argonaute family proteins can be classified into two clades, AGO and PIWI. The AGO-clade proteins are ubiquitously expressed in most organisms and associate with ~22 nucleotide (nt) microRNAs (miRNAs) or small interfering RNAs (siRNAs) to form RISCs (Siomi and Siomi, 2009; Ghildiyal and Zamore, 2009; Czech and Hannon, 2011; Meister, 2013). The RISCs repress the expression of their target genes and regulate a wide variety of biological processes (Okamura and Lai, 2008). In contrast, the PIWI-clade proteins are primarily expressed in animal gonads and associate with ~23–33 nt PIWI-interacting RNAs (piRNAs) to form piRNA-induced silencing complexes (piRISCs) (Malone and Hannon, 2009; Weick and Miska, 2014; Iwasaki et al., 2015; Czech and Hannon, 2016). The piRISCs repress the expression of transposable elements and thus contribute to the maintenance of genome integrity. There are notable differences between the RISC and piRISC assembly processes. During the RISC assembly, a small RNA duplex is loaded onto the AGO protein (Kobayashi and Tomari, 2016). Subsequently, one strand of the duplex (the passenger strand) is selectively discarded, and the other strand (the guide strand) remains bound to the AGO protein to form the mature RISC. In contrast, during the piRISC assembly, a long single-stranded piRNA intermediate is initially loaded onto the PIWI protein, with its 5′ end anchored within the protein. Subsequently, the piRNA intermediate in the PIWI protein is cleaved on the 3′ downstream side by the endonuclease Zucchini (MitoPLD in mouse) to form a precursor piRNA (pre-piRNA) (Ipsaro et al., 2012; Nishimasu et al., 2012; Han et al., 2015; Mohn et al., 2015; Homolka et al., 2015). Any extra 3′ nucleotides of the pre-piRNA bound to the PIWI protein are trimmed by the exonucleases Nibbler (Feltzin et al., 2015; Wang et al., 2016) and/or Trimmer (Izumi et al., 2016; Tang et al., 2016). The piRNA 3′ end is then 2′-*O*-methylated by Hen1 (also known as Pimet) to increase its stability (Horwich et al., 2007; Saito et al., 2007).

Previous structural studies of the prokaryotic and eukaryotic AGO-clade proteins provided mechanistic insights into RISC-mediated RNA silencing. The crystal structures of *Pyrococcus furiosus* AGO (Song et al., 2004) and *Aquifex aeolicus* AGO (Yuan et al., 2005) in their apo states revealed that Argonaute adopts a bilobed architecture, comprising four signature domains (N, PAZ, MID, and PIWI) and two linker domains (L1 and L2), and that the PIWI domain adopts an RNase H fold and is responsible for target cleavage. Subsequently, the crystal structures of *Thermus thermophilus* AGO (TtAgo) bound to a guide strand (Wang et al., 2008a) and bound to guide and target strands (Wang et al., 2008b, 2009; Sheng et al., 2014) provided mechanistic insights into the guide-target recognition and the subsequent target cleavage. The TtAgo structures showed that the

5′ and 3′ ends of the guide are anchored within the MID-PIWI and PAZ domains, respectively. More recently, the crystal structures of eukaryotic AGOs bound to a guide RNA, such as *Kluyveromyces polysporus* Argonaute (KpAgo) (Nakanishi et al., 2012), human Argonaute2 (hAgo2) (Schirle and MacRae, 2012; Elkayam et al., 2012), and human Argonaute1 (hAgo1) (Faehnle et al., 2013; Nakanishi et al., 2013), have been reported. These structures highlighted the structural differences between the eukaryotic and prokaryotic AGOs, such as the eukaryotic-specific insertions, despite their overall structural similarity. Furthermore, a series of crystal structures of hAgo2 bound to a guide RNA and a target RNA revealed the conformational changes in the protein accompanying the guide-target base pairing (Schirle et al., 2014). Single-molecule imaging studies further illuminated the structural dynamics of target recognition and cleavage by mammalian Ago2 (Chandradoss et al., 2015; Jo et al., 2015; Salomon et al., 2015) and *Drosophila* Ago2 (Yao et al., 2015). In stark contrast to the AGO-clade Argonautes, structural information is still limited for the PIWI-clade Argonautes. Although the structures of the PAZ domain (Zeng et al., 2011; Tian et al., 2011; Simon et al., 2011) and the MID domain (Cora et al., 2014) of the mammalian PIWI proteins are available, the structures of full-length PIWI-clade Argonautes remain unresolved, primarily because of difficulties in sample preparation for structural analysis.

BmN4 cells, a *Bombyx mori* ovary-derived cultured cell line, express two PIWI proteins, Siwi and BmAgo3 (Kawaoka et al., 2009), and are widely used as a cultured cell model for investigating the mechanisms underlying the piRNA pathway. In the secondary piRNA biogenesis pathway (also known as the ping-pong cycle) (Brennecke et al., 2007; Gunawardane et al., 2007; Czech and Hannon, 2016), antisense piRNA-bound Siwi and sense piRNA-bound BmAgo3 reciprocally cleave complementary transcripts, to couple the amplification of piRNAs with the repression of transposable elements (Kawaoka et al., 2009; Xiol et al., 2014; Nishida et al., 2015). In this process, Siwi requires the ATP-dependent RNA unwinding activity of the DEAD-box RNA helicase BmVasa, for the release of the cleavage products (5′ and 3′ cleavage products) (Nishida et al., 2015). This mechanism ensures the transfer of the 3′ cleavage products from Siwi to BmAgo3, thereby facilitating the ping-pong cycle (Xiol et al., 2014; Nishida et al., 2015).

In this study, we purified the endogenous Siwi-piRISC from BmN4 cells, using a monoclonal anti-Siwi antibody (Nishida et al., 2015), and determined its crystal structure at 2.4 Å resolution. The structure reveals that Siwi adopts a bilobed architecture consisting of the N-PAZ and MID-PIWI lobes, with the 5′ and 3′ ends of the co-purified endogenous piRNA anchored at the MID-PIWI interface and the PAZ domain, respectively. Our structure-guided mutational analyses confirm that the anchoring of both ends of the piRNA is important for stable piRISC formation and reveal that the catalytic tetrad in the PIWI domain is responsible for target cleavage. A structural comparison of Siwi and hAgo2 revealed notable differences in the arrangement of the N-PAZ lobes with respect to the MID-PIWI lobes, resulting in the structural differences in their central channels that accommodate the guide and target RNAs. Collectively, the present structure provides critical information toward a mechanistic understanding of piRISC-mediated transposon silencing.

RESULTS

Preparation of the Siwi-piRISC

We prepared Sepharose beads conjugated with the anti-Siwi antibody (Nishida et al., 2015) and set out to purify the endogenous Siwi-piRISC from BmN4 cells for crystallization. Importantly, previous studies showed that the hAgo2-RISC, but not the small RNA-free hAgo2, is resistant to protease (thermolysin) digestion (Elkayam et al., 2012) and that the anti-Siwi antibody recognizes the N-terminal intrinsically disordered region of Siwi (Nishida et al., 2015). Based on these observations, we hypothesized that the Siwi-piRISC core is also resistant to protease treatment and could be separated from the anti-Siwi antibody beads by the protease digestion of the N-terminal disordered region of Siwi (Figure S1A). To test this hypothesis, we immunoisolated the Siwi-piRISC from BmN4 lysates using the anti-Siwi antibody beads, treated the complex with thermolysin, and then analyzed the supernatant by SDS-PAGE. Whereas the immunoisolated full-length Siwi (101 kDa) migrated as an ~100-kDa band on the gel, an ~80-kDa single band was liberated in the supernatant after the thermolysin treatment (Figure S1B). An N-terminal sequence analysis revealed that the ~80-kDa fragment begins with Ile130 of Siwi, suggesting that it corresponds to the stable core region (residues 130–899) of Siwi. The Siwi core region was further purified by chromatography on heparin and size-exclusion columns and was eluted as a single peak from the size-exclusion column (Figures S1C and S1D). Absorbances at 260 and 280 nm of the peak indicated that the purified Siwi associates with nucleic acids (Figure S1C). ^{32}P-end labeling of the RNAs isolated from the fraction revealed that 28- to 30-nt RNAs are associated with Siwi (Figure S1E), consistent with our previous observation (Nishida et al., 2015). Together, these results indicate that the purified sample represents the mature Siwi-piRISC core, which lacks its N-terminal flexible region.

Overall Structure of the Siwi-piRISC

We crystallized the purified Siwi-piRISC and determined its structure at 2.4 Å resolution, by molecular replacement using the hAgo2 structure (PDB: 4OLA) (Schirle and MacRae, 2012) as the search model (Table S1). The structure revealed that Siwi (residues 130–899) consists of four domains (N, PAZ, MID, and PIWI) and three linker domains (L0, L1, and L2) (residues 130–167 are referred to as L0) and can be divided into two lobes (N-PAZ and MID-PIWI) (Figures 1A and 1B). The N-PAZ lobe consists of the L0 (residues 157–167), N (residues 168–240), L1 (residues 241–317), PAZ (residues 318–426), and L2 (residues 427–484) domains, whereas the MID-PIWI lobe consists of the L0 (residues 130–156), L2 (residues 485–527), MID (residues 528–657), and PIWI (residues 658–899) domains. The L0 region contains two β strands and interacts with the β strands in the L1, L2, and PIWI domains, thereby contributing to the integration of the two lobes (Figure 1B). Siwi has a nucleic-acid-binding channel between the two lobes, in which electron densities are observed for the co-purified endogenous RNAs (Figure S2A), as in the crystal structures of the eukaryotic AGOs (Schirle and MacRae, 2012; Nakanishi et al., 2012; Faehnle et al., 2013; Nakanishi et al., 2013). The electron density for the 5′ nucleotide

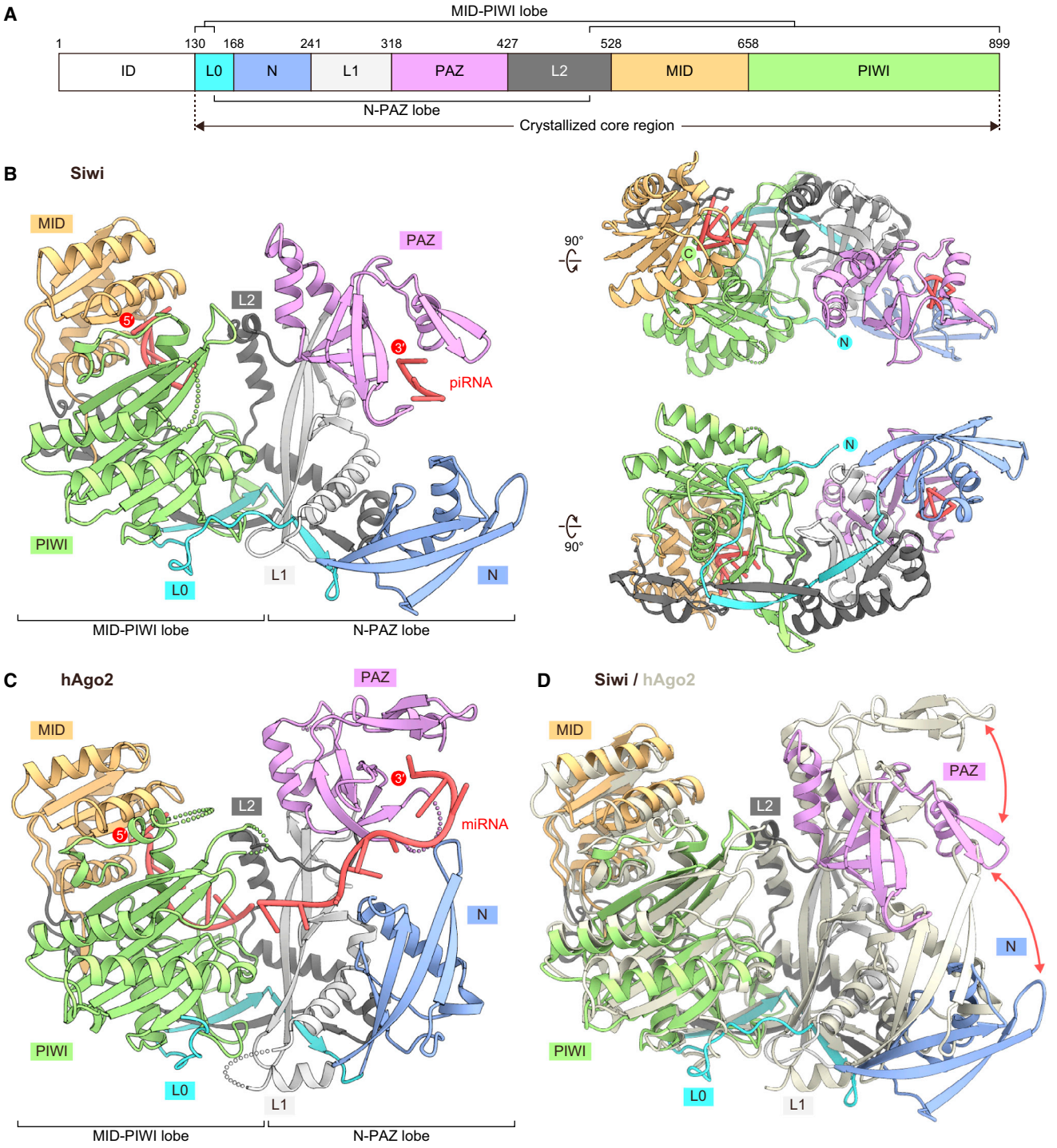

Figure 1. Overall Structure

(A) Domain organization of Siwi. ID, intrinsically disordered region.

(B) Crystal structure of the Siwi-piRISC. Top and bottom views are shown on the right.

(C) Crystal structure of the hAgo2-RISC (PDB: 4W5N) (Schirle et al., 2014).

(D) Superimposition of Siwi (colored) and hAgo2 (PDB: 4W5N) (beige). Structural differences in their N and PAZ domains are indicated by red arrows.

See also Figures S1 and S2 and Table S1.

could be fitted to a uridine (Figure S2B), consistent with the preference of Siwi for the U1 nucleotide in the guide piRNA (g1U bias) (Kawaoka et al., 2009, 2011; Xiol et al., 2014; Nishida et al., 2015). The electron density was observed for the 2′-*O*-methyl group in the 3′ nucleotide (Figure S2C), consistent with earlier observations that mature piRNAs possess the 2′-*O*-methylated 3′ end (Horwich et al., 2007; Saito et al., 2007; Kawaoka et al., 2011). Since the Siwi-bound endogenous piRNAs have divergent sequences and lengths (predominantly 28-nt long) (Kawaoka et al., 2009; Nishida et al., 2015), we modeled 1-UAUUU-5 and 26-UUU$_m$-28 (U$_m$ indicates the 2′-*O*-methylated U) as the 5′ and 3′ segments of the bound piRNA, respectively, according to the size and shape of their nucleobases. No electron density was observed for the middle segment (nucleotides 6–25) of the piRNA, as in the guide-bound eukaryotic AGO structures (Schirle and MacRae, 2012; Nakanishi et al., 2012, 2013; Elkayam et al., 2012; Faehnle et al., 2013), suggesting that the middle region is disordered in the present structure. Together, these observations indicate that the present structure represents the Siwi-piRISC bound to mature piRNAs.

Structural Comparison between Siwi and hAgo2

A structural comparison between Siwi and hAgo2 (Schirle and MacRae, 2012; Elkayam et al., 2012; Schirle et al., 2014) revealed unexpected similarities and differences between the PIWI and AGO proteins (Figures 1B–1D). The individual domains of Siwi and hAgo2 can be superimposed (root-mean-square deviation of 0.9–2.0 Å for equivalent Cα atoms) (Figure S3A), although they share limited sequence identities (13%–32%) (Figure S4). However, there are notable differences in the arrangement of their N and PAZ domains relative to the rest of the protein (Figure 1D). In addition, the relative arrangement between their N and PAZ domains differs between Siwi and hAgo2 (Figure S3B). These distinctive arrangements are stabilized by extensive interactions at their N-L1-L2 and L1-PAZ-L2 interfaces (Figure 2).

At the N-L1-L2 interface of Siwi, Trp166 in the L0 domain and Trp477 in the L2 domain form a hydrophobic core with residues from the N domain (Leu168, Leu200, Tyr207, and Val209) and the L1 domain (Tyr247, Phe251, and Ile254), thereby playing a central role in the formation of the N-L1-L2 interface (Figures 2A and 2B). Notably, Trp477 of Siwi is conserved among the PIWIs, but not among the AGOs, in which the equivalent residue is conserved as phenylalanine (Phe397 in hAgo2) (Figure S5). In the hAgo2 structure (Schirle et al., 2014), Phe397 forms a hydrophobic core with residues from the N domain (Ile54, Val93, Tyr101, and Ala103) and the L1 domain (Val165), in a manner distinct from that of Siwi Trp477 (Figures 2D and 2E). In addition, hAgo2 has an AGO-specific α-helix (referred to as AGO-Ins) between the N and L1 domains that contributes to the N-L1 interface formation (Figures 2D, 2E, and S5).

In the L1-PAZ-L2 interface of Siwi, four β strands (β8, β9, β11, and β12) in the L1 domain and three β strands (β13, β14, and β19) in the PAZ domain form a seven-stranded β-barrel-like structure, which is stabilized by a hydrophobic core formed by residues from the L1 domain (Met267, Phe272, Pro274, Trp288, Lys311, and Leu313) and the PAZ domain (Met347, Thr354, and Thr426) (Figures 2A and 2C). This β-barrel-like structure fixes the arrangement between the L1 and PAZ domains. The Met347/Thr354 and Leu313 residues of Siwi are replaced with Glu268/Lys278 and Phe224 in hAgo2, respectively, and the AGOs have a conserved proline residue (Pro229 in hAgo2) in the L1 domain (Figure S5). These residues of hAgo2 appear to prevent the L1 and PAZ domains from forming a β barrel-like structure (Figures 2D and 2F). Instead, hAgo2 has Tyr225 in the last β strand (β12) of the L1 domain, which forms a hydrophobic core with residues from the PAZ domain (Leu265 and Phe233) and the L2 domain (Gln350 and Cys352) (Figure 2F). In addition, the L1-PAZ-L2 interface is reinforced by polar interactions between Arg196 (L1) and Glu261 (PAZ), and between Gln350 (L2) and Lys266 (PAZ) (Figure 2F). The Phe224/Pro229/Gln350 and Arg196/Tyr225/Glu261 residues of hAgo2 are strictly and highly conserved among the AGOs, but not among the PIWIs, respectively (Figure S5). Indeed, these interactions at the L1-PAZ-L2 interface are conserved in hAgo1 (Faehnle et al., 2013; Nakanishi et al., 2013). Together, these structural observations highlight the distinct spatial arrangements of the N and PAZ domains relative to the L1-L2 domains between the AGO- and PIWI-clade Argonautes.

Recognition of the 5′ Phosphate of the piRNA

The 5′ end of the piRNA is flipped into a binding pocket at the interface between the MID and PIWI domains (Figure 3A). The 5′ phosphate is recognized by the main-chain amide group of Val624 and the side chains of Tyr607, Lys611, Gln623, and Lys649 (Figure 3A). We observed a strong electron density in the vicinity of the 5′ phosphate; we modeled it as a Mg^{2+} ion, based on its octahedral geometry and coordination distances (~2.1 Å) (Figure S6A). The Mg^{2+} ion was likely co-purified from the BmN4 cells, since the purification and crystallization buffers lacked divalent cations. The Mg^{2+} ion is octahedrally coordinated by phosphates 1 and 3 in the piRNA, the side chain of Gln645, the C-terminal carboxylate group of Leu899, and a water molecule (Figure 3A). To examine the functional importance of the residues involved in the 5′ phosphate recognition, we expressed the FLAG-tagged, wild-type and mutants of Siwi in BmN4 cells, immunopurified the Siwi proteins, and then analyzed the Siwi-bound piRNAs (Figure 3B). The K611A, Q623A, Q645A, and K649A mutants were associated with substantially reduced levels of piRNAs, as compared with wild-type Siwi. These results confirmed the importance of the 5′ phosphate recognition for piRNA loading, consistent with previous studies (Kawaoka et al., 2011; Cora et al., 2014). Tyr607, Lys611, Gln623, Gln645, and Lys649 are strictly conserved among the PIWI-clade proteins (Figure S5), indicating the conservation of the metal-dependent recognition mechanism of the piRNA 5′ phosphate among them. Notably, Gln645 of Siwi is replaced with a lysine in the eukaryotic AGOs (Lys566 of hAgo2) (Figure S5), and Lys566 interacts with phosphates 1 and 3 of the guide RNA in the hAgo2 structure (Schirle and MacRae, 2012; Elkayam et al., 2012) (Figures 3C and 3D). In contrast, in the TtAgo structure, phosphates 1 and 3 in the guide are recognized by the protein in a metal-dependent manner with the Mg^{2+} ion held by Gln433, which is equivalent to Gln623 of Siwi (Gln645 of Siwi is replaced with Gly453 in TtAgo) (Sheng et al., 2014) (Figure 3E). These structural findings indicate that the PIWIs and prokaryotic AGOs recognize the 5′ phosphate of

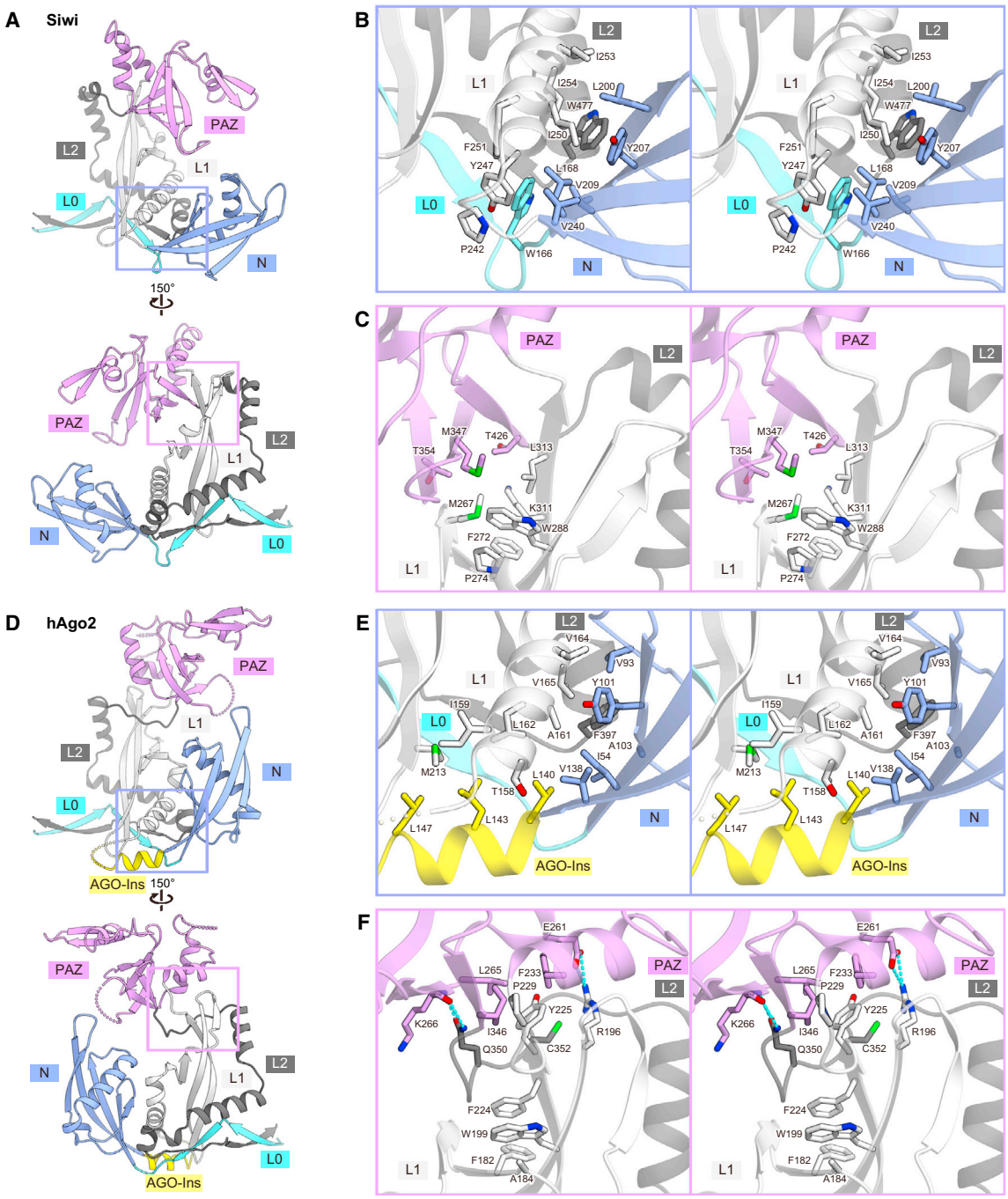

Figure 2. N-PAZ Lobe

(A) N-PAZ lobe of Siwi.

(B and C) N-L1-L2 (B) and L1-PAZ-L2 (C) interfaces of Siwi (stereoviews).

(D) N-PAZ lobe of hAgo2 (PDB: 4W5N) (Schirle et al., 2014).

(E and F) N-L1-L2 (E) and L1-PAZ-L2 (F) interfaces of hAgo2 (PDB: 4W5N) (stereoviews). The AGO-specific insertion is highlighted in yellow.

See also Figures S3, S4, and S5.

the guide strand in metal-dependent manners, whereas the eukaryotic AGOs neutralize the negative charge of the 5′ phosphate via a conserved lysine residue.

Recognition of g1U of the piRNA

The U1 nucleotide in the piRNA (g1U) is recognized in a base-specific manner by a loop region between the third β strand

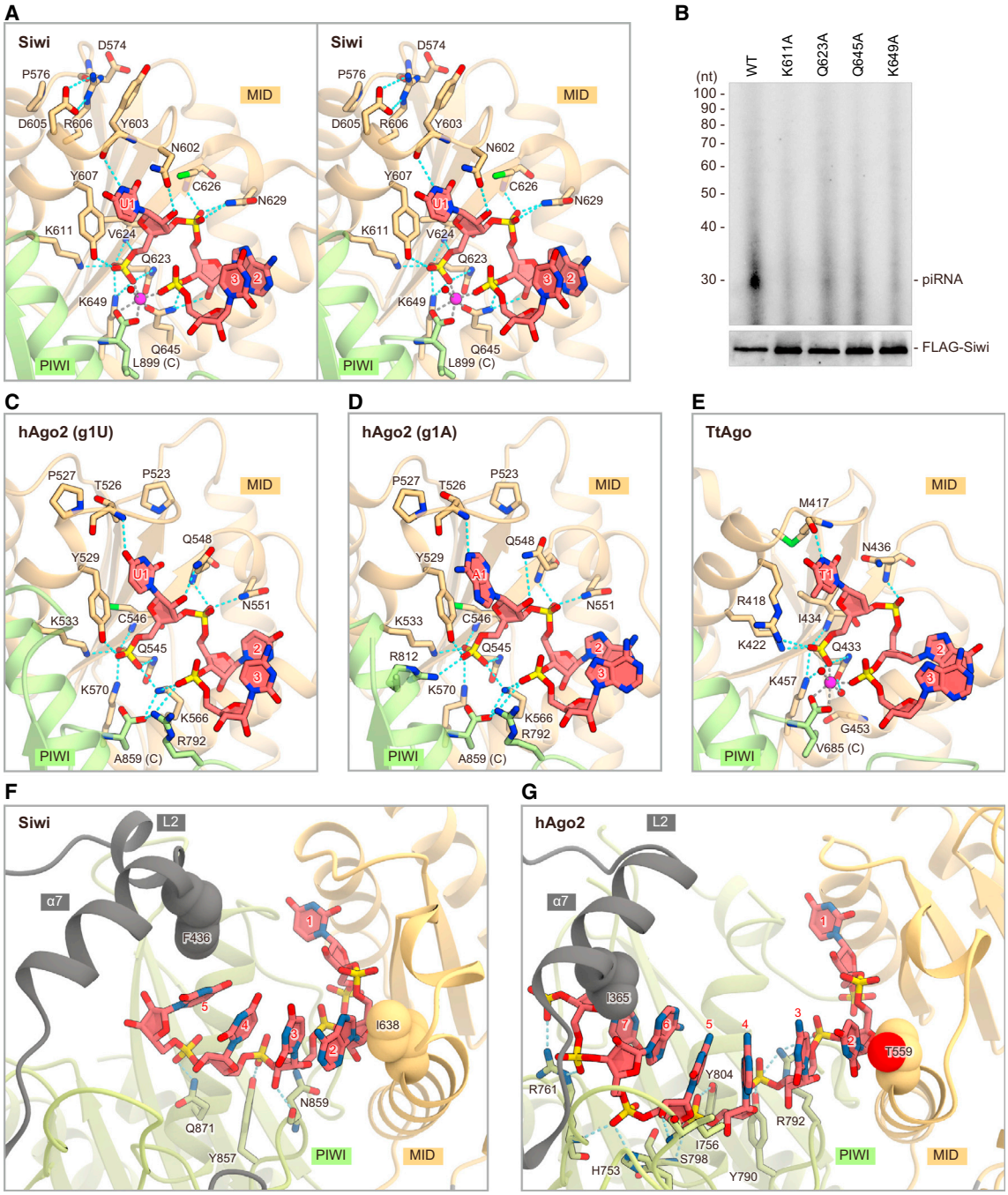

Figure 3. Recognition of the piRNA 5′ Segment

(A) Recognition of the piRNA 5′ segment by Siwi (stereoview). The bound Mg^{2+} ion and water molecule are shown as magenta and red spheres, respectively. Hydrogen bonding and electrostatic interactions are indicated by cyan dashed lines. Coordinations to the Mg^{2+} ion are shown as gray dashed lines.

(B) piRNA loading in the wild-type and mutants of Siwi. FLAG-Siwi was used as a loading control.

(C–E) Recognition of the guide 5′ segment by hAgo2 (g1U; PDB: 4W5O) (C), hAgo2 (g1A; PDB: 4OLA) (D), and TtAgo (g1T; PDB: 4NCB) (E). In (E), the bound Mg^{2+} ion is shown as a magenta sphere.

(F and G) Recognition of the seed region in the guide RNA by Siwi (F) and hAgo2 (PDB: 4W5N) (G).

See also Figure S6 and Table S2.

and the third α-helix in the MID domain (known as the specificity loop [Frank et al., 2010]) (Figure 3A). The N3 of the U1 forms a hydrogen bond with the main-chain carbonyl group of Tyr603 in the specificity loop, and its nucleobase stacks with the side chain of Tyr607 (Figure 3A). The conformation of the specificity loop appears to be stabilized by stacking interactions between Pro576-Arg606-Tyr603, with Arg606 forming salt bridges with Asp574 and Asp605 (Figure 3A). Modeling indicated a steric clash or charge repulsion between Tyr603 in the specificity loop and the modeled A, G and C (Figure S6B), thus explaining the g1U bias of Siwi (Kawaoka et al., 2009, 2011; Xiol et al., 2014; Nishida et al., 2015). The residues in the specificity loop differ between Siwi and BmAgo3 (Figure S5), consistent with the observation that, unlike Siwi, BmAgo3 lacks the preference for the piRNA 5′ nucleotide (Kawaoka et al., 2009, 2011; Nishida et al., 2015). Although *Drosophila* Piwi and Aubergine also prefer g1U (Brennecke et al., 2007), the residues in their specificity loops differ from those in Siwi (Figure S5). Thus, further structural studies are required to elucidate their g1U recognition mechanisms. hAgo2 preferentially binds g1U and g1A (Frank et al., 2010; Elkayam et al., 2012), and g1U or g1A is accommodated within a pocket defined by the specificity loop in the hAgo2 structure (Frank et al., 2010; Schirle and MacRae, 2012; Elkayam et al., 2012; Schirle et al., 2014) (Figures 3C and 3D). The specificity loop of hAgo2 contains Pro523, Gly524, and Pro527, which are highly conserved among the eukaryotic AGOs, but not among the PIWIs (Figure S5); it adopts a conformation distinct from that of Siwi (Figures 3C and 3D). Together, these structural observations reinforce the notion that the preference for the guide 5′ nucleotide is primarily defined by the specificity loop in the MID domain.

Recognition of the Seed Region of the piRNA

In the Siwi structure, nucleotides 2–5 of the piRNA adopt a nearly A-form conformation (Figure S6C), and are bound to a narrow groove formed by the L2, MID and PIWI domains (Figures 3F and S6D), as in the eukaryotic AGOs (Schirle and MacRae, 2012; Nakanishi et al., 2012, 2013; Elkayam et al., 2012; Faehnle et al., 2013). This structural feature indicated that, as in the AGOs, nucleotides 2–5 (the seed region) in the piRNA serve as a nucleation site for base pairing with a target RNA. Base 2 interacts with Ile638 in the MID domain, whereas phosphates 4 and 5 are recognized by Tyr857 and Gln871 in the PIWI domain, respectively (Figure 3F). The 2′-OH group of nucleotide 3 interacts with the main-chain carbonyl group of Asn859. In addition, base 5 interacts with Phe436 in helix α7 in the L2 domain (Figure 3F), indicating that the base stacking between nucleotides 5 and 6 would be interrupted. In the guide-bound hAgo2 structure (Schirle and MacRae, 2012; Elkayam et al., 2012; Schirle et al., 2014), Ile365 in helix α7, which is equivalent to helix α7 in Siwi, is inserted between nucleotides 6 and 7 of the guide RNA, thereby inducing a pronounced kink in the guide strand (Figure 3G). Moreover, a comparison between the guide-bound and guide-target-bound hAgo2 structures revealed that helix α7 in the L2 domain is displaced outward upon guide-target base pairing, thus widening the nucleic-acid-binding channel (Schirle et al., 2014). Phe436 of Siwi is conserved among the PIWIs, but not among the AGOs, whereas Ile365 of hAgo2 is conserved among the AGOs, but not among the PIWIs (Figure S5). These observations imply that Phe436 of Siwi and Ile365 of hAgo2 play similar roles in inducing a kink in the guide RNA within the binary complex. Together, these structural findings suggest that, as in mammalian Ago2 (Chandradoss et al., 2015; Jo et al., 2015; Salomon et al., 2015), Siwi primarily uses a small region (nucleotides 2–5) of the piRNA guide to interrogate their target sites, and the propagation of the guide-target pairing induces the widening of the nucleic-acid-binding channel.

Recognition of the 3′ End of the piRNA

The 3′ end of the piRNA is anchored within a binding pocket in the PAZ domain (Figure 4A). The 2′-OH and phosphate groups of nucleotide 27 interact with Tyr355 and Lys386, respectively (Figure 4B). Base 28 forms a stacking interaction with Phe370, and phosphate 28 is extensively recognized by Tyr350, Tyr355, Tyr382 and Tyr387 (Figure 4B). The 3′-OH group and the 2′-oxygen atom of nucleotide 28 form hydrogen bonds with Tyr383/Tyr417 and Tyr417, respectively (Figure 4B). Importantly, the 2′-*O*-methyl group of nucleotide 28 is accommodated within a hydrophobic pocket formed by Phe370, Tyr379 and Tyr417 (Figure 4C), as in the isolated PAZ domains from Hiwi1 (Tian et al., 2011) and Miwi (Simon et al., 2011) (Figures S7A–S7C). The Y350A/Y382A and F370A/Y379A mutations substantially reduced the piRNA loading (Figure 4D), confirming the importance of the recognition of the 2′-*O*-methylated piRNA 3′ end in this process. This result is consistent with a previous observation that Siwi-bound piRNAs are stabilized by Hen1-mediated 2′-*O*-methylation (Izumi et al., 2016). Tyr379 of Siwi is conserved as a tyrosine or a phenylalanine among the PIWIs (Phe342 of Hiwi1 and Phe343 of Miwi) (Figure S5), and contributes to creating the spacious pocket for the 2′-*O*-methyl group (Figures 4C and S7A–S7C). hAgo2 has a restricted 3′-nucleotide-binding pocket (Figure 4E and S7D), as compared to those of the PIWIs, since Tyr379 of Siwi is replaced with a smaller valine residue in the AGOs (Val308 of hAgo2) (Figure S5). Together, these findings highlight the functional importance of the spacious 3′-nucleotide-binding pocket of the PIWI-clade PAZ domains.

Potential t1A-Binding Pocket

Eukaryotic AGO proteins, such as hAgo2 (Lewis et al., 2005), and a subset of PIWI proteins, such as Siwi and *Drosophila* Aubergine (Wang et al., 2014), prefer target RNAs with an adenine at the position opposite the first nucleotide in their guide RNAs (referred to as t1A). The guide-target-bound hAgo2 structures revealed that the t1A nucleotide is accommodated within a binding pocket at the L2-MID interface (Schirle et al., 2015) (Figure 5A). The N6 of t1A forms a hydrogen bond with the side chain of Ser561, whereas the N1 and N6 atoms of t1A form a water-mediated hydrogen-bonding network with Met437, Asn439, Lys440, and Ile477. In addition, the t1A nucleobase forms a stacking interaction with the side chain of Arg438.

The present structure revealed that Siwi has a potential t1A-binding pocket similar to that of hAgo2 (Figure 5B). However, in the Siwi structure, the t1A-binding pocket is not fully accessible, as the side chain of Arg520, equivalent to Arg438 in hAgo2, adopts a distinct conformation (Figure 5B). It is

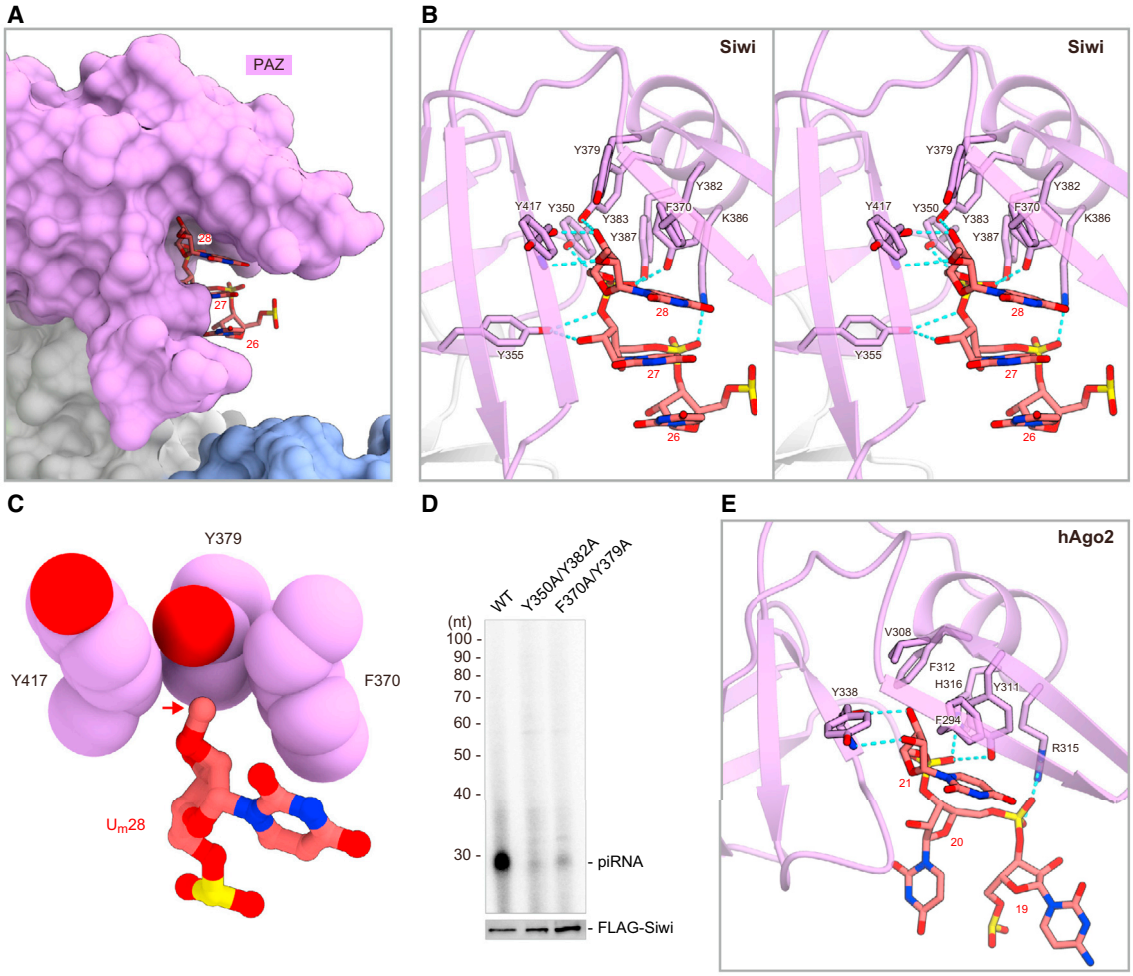

Figure 4. Recognition of the piRNA 3′ Segment

(A) Binding of the piRNA 3′ end to the Siwi-PAZ domain.

(B) Recognition of the piRNA 3′ segment by the Siwi-PAZ domain (stereoview). Hydrogen bonding and electrostatic interactions are indicated by cyan dashed lines.

(C) Recognition of the 2′-*O*-methylated piRNA 3′ end. The 2′-*O*-methyl group is indicated by a red arrow.

(D) piRNA loading in the wild-type and mutants of Siwi. FLAG-Siwi was used as a loading control.

(E) Recognition of the miRNA 3′ segment by the hAgo2-PAZ domain (PDB: 4W5N).

See also Figure S7 and Table S2.

thus likely that Arg520 undergoes a conformational change to accommodate the t1A nucleotide. Ser561 of hAgo2 is replaced with a threonine in Siwi (Thr640) and *Drosophila* Aubergine, whereas it is replaced with a bulkier glutamine in BmAgo3 and *Drosophila* Ago3 (Figure S5), suggesting that the t1A binding pocket is occluded by the glutamine residues in BmAgo3 and *Drosophila* Ago3, which lack the t1A preference.

Catalytic Tetrad in the PIWI Domain

The crystal structures of the eukaryotic and prokaryotic AGOs revealed that the PIWI domains adopt an RNase H fold, with the DEDX catalytic tetrad (X is generally Asp or His) in the active site (Figure 6A–6D). The catalytic tetrad was originally discovered in the KpAgo structure, in which the DEDD tetrad is formed by the DDD triad (Asp974, Asp1046, and Asp1198) and the glutamate finger (Glu1013) on a loop region (referred to as PIWI domain loop 2) between the third β strand and the first α-helix in the RNase H fold (Nakanishi et al., 2012) (Figure 6A). In the hAgo2 structure, the DEDH tetrad is formed by the DDH triad (Asp597, Asp669 and His807) and the glutamate finger (Glu637) (Schirle and MacRae, 2012; Elkayam et al., 2012) (Figure 6B). hAgo1 also has a catalytic tetrad similar to that of hAgo2 (Faehnle et al., 2013; Nakanishi et al., 2013). In the guide-bound TtAgo structure, PIWI domain loop 2 is disordered (the "unplugged" conformation), whereas in the guide-target bound structure, the loop region becomes ordered and the glutamate finger (Glu512) is inserted within the DDH triad to complete the catalytic tetrad (the "plugged-in" conformation) (Sheng et al., 2014) (Figures 6C and 6D). Thus, unlike the eukaryotic AGOs, the guide-target base pairing induces the "unplugged"

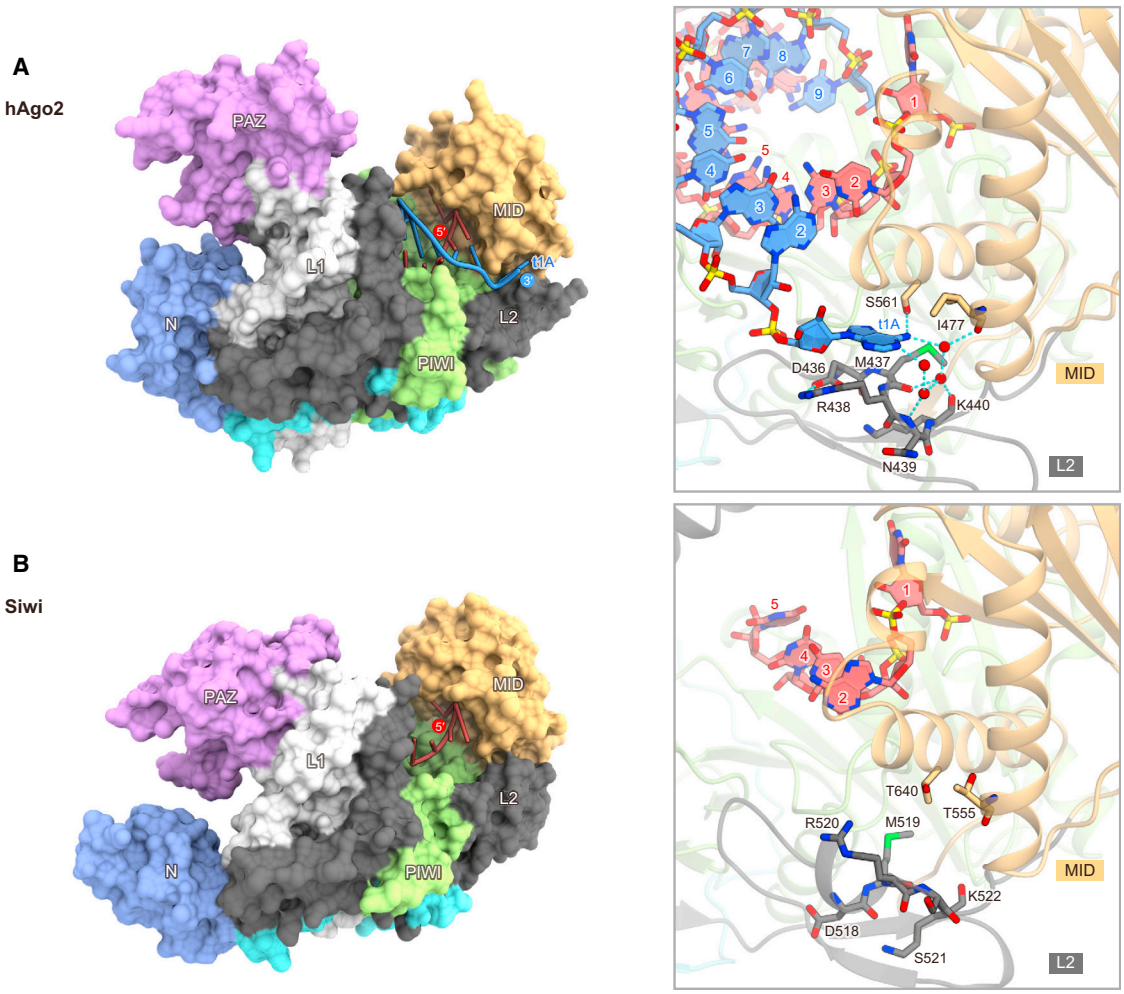

Figure 5. t1A-Binding Pocket

(A and B) t1A-binding pockets of hAgo2 (PDB: 4W5O) (A) and Siwi (B). Surface and ribbon representations of the t1A-binding pocket are shown in the left and right panels, respectively. Water molecules are shown as red spheres. Hydrogen bonds are indicated by cyan dashed lines.

to "plugged-in" conformational changes in TtAgo. In these eukaryotic and prokaryotic AGO structures, the plugged-in conformation is stabilized through a conserved hydrogen-bonding network within the PIWI domain (Figure 6A–6C).

The present structure provides the first structural insight into the PIWI domain of PIWI-clade Argonautes and reveals that the PIWI domain of Siwi adopts an RNase H fold similar to those of the AGO-clade Argonautes (Figure 6E). In addition, the residues involved in the formation of the catalytic tetrad (Asp670, Glu708, Asp740, and His874 in Siwi) and the hydrogen-bonding network (His673, Ser681, Arg739, and Glu754 in Siwi) are conserved among the PIWI-clade Argonautes (Figure S5). Indeed, like the D670A, D740A, and H874A mutations, the E708A mutation of Siwi abolished the slicer activity (Figure 6F), indicating that Glu708 participates in the catalytic-tetrad formation. However, in the present Siwi structure, PIWI domain loop 2 (residues 704–708) is disordered, and thus Glu708 adopts the unplugged state, although the other active-site residues are located at positions similar to those of hAgo2 (Figure 6E). These observations suggest that, as in TtAgo, the catalytic tetrad of Siwi becomes completed via a conformational change following guide-target base pairing.

DISCUSSION

In this study, we affinity-purified the endogenous Siwi-piRISC from BmN4 cells and determined its crystal structure at 2.4 Å resolution. The Siwi-piRISC structure reveals the mechanism by which Siwi recognizes the g1U and the 2′-*O*-methylated 3′ end in the piRNA guide. Our structural and mutational analyses further demonstrate that the catalytic tetrad in the PIWI domain is critical for the slicer activity of Siwi, thereby suggesting that the catalytic tetrad is a conserved feature among the AGO- and PIWI-clade Argonautes. Unlike the guide-bound eukaryotic AGO structures, the Siwi-piRISC structure adopts the unplugged conformation, as in the guide-bound TtAgo structure. The present structure also reveals that, unexpectedly, Siwi recognizes the 5′ phosphate of the piRNA in a metal-dependent manner,

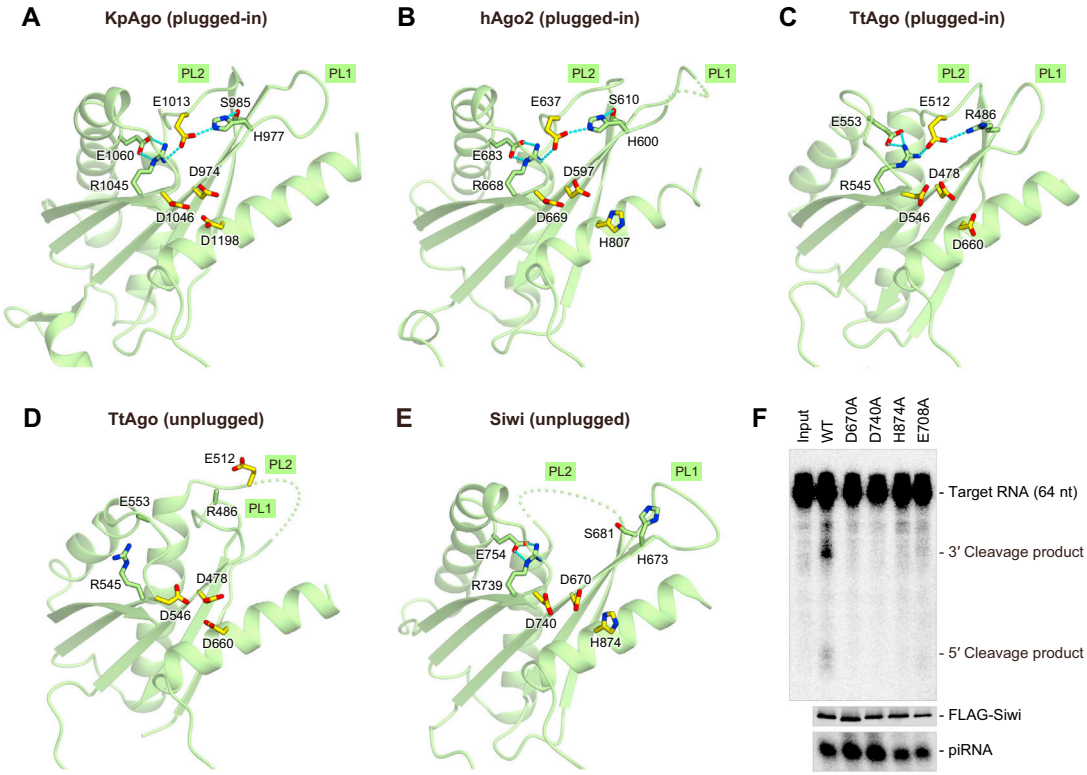

Figure 6. Catalytic Tetrad

(A–E) Catalytic tetrads in the PIWI domains of KpAgo (PDB: 4F1N) (A), hAgo2 (PDB: 4W5N) (B), TtAgo (plugged-in) (PDB: 4NCB) (C), TtAgo (unplugged) (PDB: 4N47) (D), and Siwi (E). The DEDX catalytic tetrads and the surrounding residues are shown as yellow and green sticks, respectively. Hydrogen bonding and electrostatic interactions are indicated by cyan dashed lines. The disordered regions are shown as dashed lines. PL, PIWI domain loop.

(F) Slicer activities of the wild-type and mutants of Siwi. Western blots for FLAG-Siwi and ^{32}P-labeled piRNAs are shown below.

See also Table S2.

as observed in prokaryotic, but not in eukaryotic, AGOs. These structural findings indicate that the eukaryotic PIWIs and the prokaryotic AGOs share unanticipated similarities in the catalytic-tetrad formation and the 5′-phosphate recognition. Most notably, the present structure reveals unexpected differences between Siwi and the eukaryotic AGOs in the arrangement of the N-PAZ lobe relative to the MID-PIWI lobe. These structural differences probably reflect the distinct lengths of their guide RNAs, as well as the mechanistic differences in RISC assembly and cleavage product release.

The Siwi-piRISC primarily contains a ~27–28-nt piRNA, whereas the hAgo2-RISC contains a ~21-nt miRNA (Xiol et al., 2014; Nishida et al., 2015). In the structure of hAgo2 bound to a 21-nt guide RNA (Schirle et al., 2014), the 5′ and 3′ ends of the guide are anchored within the binding pockets in the MID-PIWI and PAZ domains, respectively, whereas nucleotides 8–11 are disordered (Figure 7A). Nucleotides 2–7 (the seed region) adopt a helical conformation for base-pairing with the target RNA, whereas nucleotides 12–21 are bound to the N-PAZ lobe, with nucleotides 14–18 threaded through a narrow channel between the N and PAZ domains. In the present Siwi-piRISC structure, nucleotides 1–5 adopt conformations similar to those in the hAgo2-RISC structure (Figure 7B). In contrast, the rest of the Siwi-bound piRNA adopts a conformation distinct from that of the Ago2-bound miRNA, due to the structural differences in their N-PAZ channels. Importantly, the PAZ domain of Siwi contains the PIWI-specific insertion (residues 405–412; referred to as PIWI-Ins) (Figure S5), which protrudes into the N-PAZ channel and may facilitate the binding of longer piRNAs (Figure 7B). Although the precise trajectory of the bound piRNA is unknown, the structure of Siwi bound to a piRNA with a defined sequence may clarify the mechanism of piRNA recognition by Siwi, as in the case of hAgo2 (Schirle et al., 2014).

Eukaryotic AGOs bind an ~21-bp small RNA duplex and then eject the passenger strand (Czech and Hannon, 2011; Kobayashi and Tomari, 2016). In contrast, PIWIs are loaded with a single-stranded piRNA precursor, and its 3′ end is then processed by nucleases, such as Zucchini, Trimmer, and Nibbler (Czech and Hannon, 2016). In the human AGOs, the N domain (Kwak and Tomari, 2012; Schürmann et al., 2013) and the PAZ domain (Gu et al., 2012; Park and Shin, 2015) play important roles in the RISC assembly process. Thus, the observed structural differences between the N-PAZ lobes of Siwi and hAgo2 likely reflect their mechanistic differences in RISC assembly.

Cleavage of target RNAs by mammalian Ago2 (Jo et al., 2015; Salomon et al., 2015) and *Drosophila* Ago2 (Yao et al., 2015; Nishida et al., 2015) destabilizes the base pairing between the guide and target RNAs, thereby leading to the autonomous

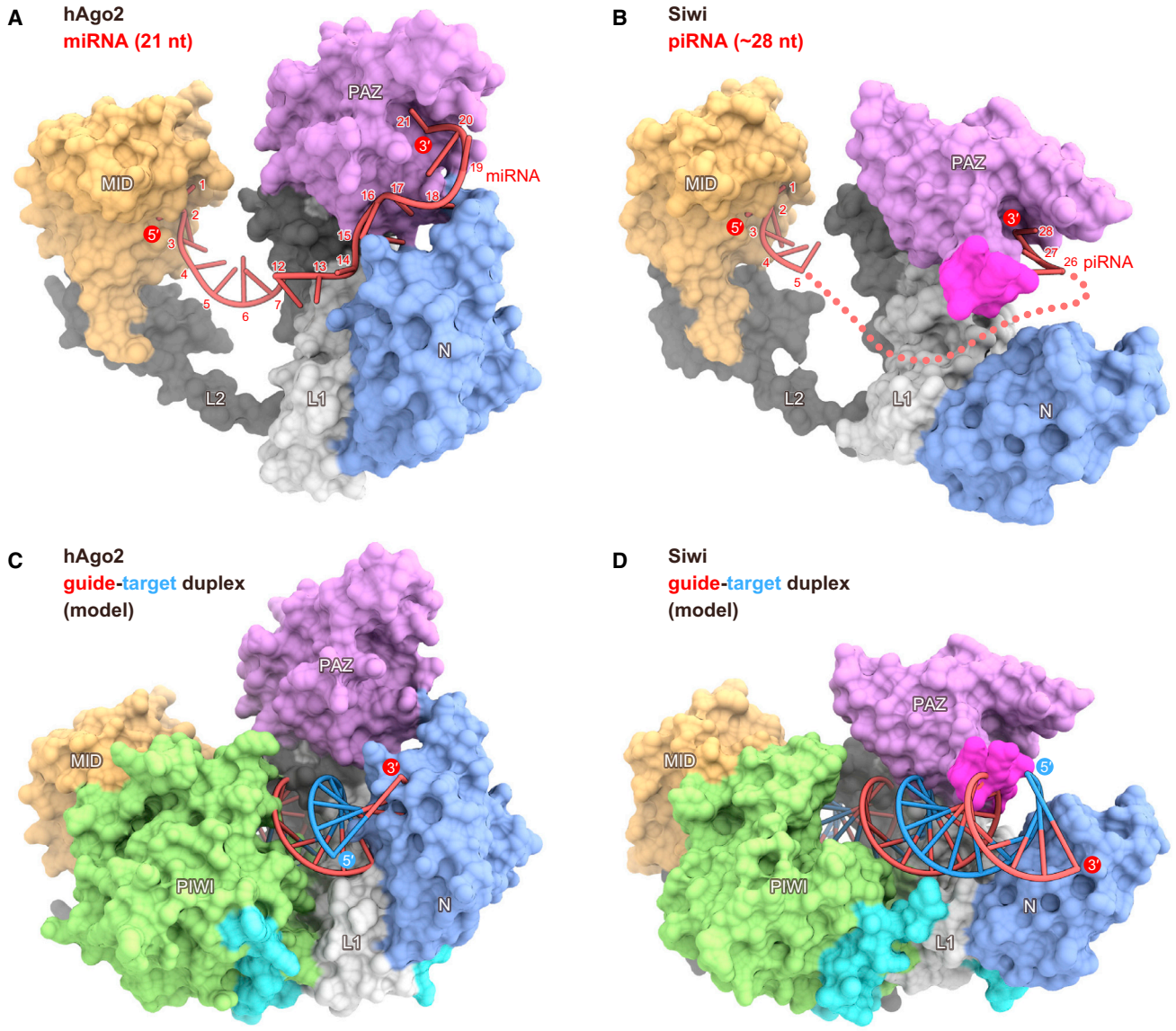

Figure 7. Nucleic-Acid-Binding Channel

(A and B) Nucleic-acid-binding channels of hAgo2 (PDB: 4W5N) (A) and Siwi (B). The L0 and PIWI domains are omitted for clarity. A possible trajectory of the bound piRNA is shown as a dotted line.

(C and D) Structures of hAgo2 (PDB: 4W5N) (C) and Siwi (D) bound to a modeled guide-target duplex. In (B) and (D), the PIWI-Ins is highlighted in magenta.

release of cleavage products. In contrast, Siwi cannot release the cleavage products autonomously and requires the DEAD-box RNA helicase BmVasa for their efficient release (Nishida et al., 2015). BmVasa associates with Siwi and BmAgo3 and facilitates the transfer of the 3′ cleavage products from Siwi to BmAgo3 in the ping-pong cycle (Xiol et al., 2014; Nishida et al., 2015). Modeling of the guide-target duplex into the hAgo2 structure indicates a steric clash between the modeled duplex and the N domain (Figure 7C), suggesting that the widening of the nucleic-acid-binding channel is required for hAgo2 to accommodate an extensively paired guide-target duplex for target cleavage, as previously proposed (Schirle et al., 2014). This outward displacement of the N-PAZ lobe probably generates an inward pressure in the hAgo2 protein, which may facilitate the product release. In contrast, the modeling of the guide-target duplex into the Siwi structure suggests that the N domain would circumvent such severe clashes; instead, it would provide favorable interactions with the duplex (Figure 7D). These structural differences might be the reasons why, after target cleavage, the nicked target strand remains bound to Siwi quite stably. As a consequence, Siwi requires BmVasa for efficient product release, in contrast to hAgo2, which releases the cleavage products autonomously. However, further structural and functional studies are needed to verify this model.

In summary, the present findings have provided a framework for understanding the mechanisms underlying piRISC-mediated

transposon silencing. As in the case of hAgo2, the structures of Siwi in complex with a piRNA and its target RNA provide mechanistic insights into target recognition and cleavage by the Siwi-piRISC. Furthermore, the structures of Siwi-piRISC bound to interactors, such as BmVasa, shed light on the mechanism by which Siwi and the interactors cooperatively function in the ping-pong cycle. Importantly, the piRISC purification strategy established here could be applicable to other PIWI proteins, when a specific antibody for an individual PIWI is available. Accumulation of structural information about other PIWIs, regardless of the species, will help to clarify the reasons why the lengths of the mature piRNAs differ among PIWI proteins from different species and why the g1U bias is not observed in the piRNAs loaded onto a subset of PIWIs, such as BmAgo3. Collectively, the present study paves the way for deciphering the molecular mechanisms of piRISC-mediated transposon silencing.

STAR★METHODS

Detailed methods are provided in the online version of this paper and include the following:

- KEY RESOURCES TABLE
- CONTACT FOR REAGENT AND RESOURCE SHARING
- EXPERIMENTAL MODEL AND SUBJECT DETAILS
  - Cell Lines
- METHOD DETAILS
  - Purification of the Siwi-piRISC
  - Crystallization and Structural Determination
  - Small RNA Isolation from the Immunopurified Siwi Complex
  - Plasmid Construction
  - In Vitro Target RNA Cleavage Assay
- QUANTIFICATION AND STATISTICAL ANALYSIS
- DATA AND SOFTWARE AVAILABILITY
  - Data Resources

SUPPLEMENTAL INFORMATION

Supplemental Information includes seven figures and two tables and can be found with this article online at http://dx.doi.org/10.1016/j.cell.2016.09.002.

AUTHOR CONTRIBUTIONS

N.M. purified and crystallized the complex and solved the structure. H.N. conceived the purification strategy using a protease, collected the diffraction data, and assisted with the structural analysis. K.S. and K.M.N. performed the mutational analysis. T.H. and H.S. established the purification strategy for endogenous PIWI-clade proteins. R.I. assisted with the structural analysis. N.M., H.N., H.S., M.C.S., and O.N. designed the experiments and wrote the manuscript. H.N., M.C.S., and O.N. supervised all of the research.

ACKNOWLEDGMENTS

We thank Akira Oe for assistance with sample preparation, Takashi Yamano for assistance with data collection, Dr. Takanori Nakane and Dr. Tomohiro Nishizawa for assistance with model building, and the beamline scientists at SPring-8 BL41XU for assistance with data collection. This research was supported by the Platform Project for Supporting in Drug Discovery and Life Science Research (Platform for Drug Discovery, Informatics, and Structural Life Science) from the Japan Agency for Medical Research and Development (AMED). H.N., K.M.N., H.S., and M.C.S. were supported by a Grant-in-Aid for Scientific Research, from the Ministry of Education, Culture, Sports, Science and Technology of Japan (26291010 and 15H01463 to H.N., 15K06948 to K.M.N., 25221003 to H.S., and 25221101 to M.C.S.). O.N. was supported by the Core Research for Evolutional Science and Technology (CREST) Program, The Creation of Basic Medical Technologies to Clarify and Control the Mechanisms Underlying Chronic Inflammation of Japan Science and Technology Agency (JST).

Received: July 22, 2016
Revised: August 29, 2016
Accepted: August 31, 2016
Published: September 29, 2016

REFERENCES

Adams, P.D., Afonine, P.V., Bunkóczi, G., Chen, V.B., Davis, I.W., Echols, N., Headd, J.J., Hung, L.W., Kapral, G.J., Grosse-Kunstleve, R.W., et al. (2010). PHENIX: a comprehensive Python-based system for macromolecular structure solution. Acta Crystallogr. D Biol. Crystallogr. *66*, 213–221.

Brennecke, J., Aravin, A.A., Stark, A., Dus, M., Kellis, M., Sachidanandam, R., and Hannon, G.J. (2007). Discrete small RNA-generating loci as master regulators of transposon activity in *Drosophila*. Cell *128*, 1089–1103.

Chandradoss, S.D., Schirle, N.T., Szczepaniak, M., MacRae, I.J., and Joo, C. (2015). A dynamic search process underlies microRNA targeting. Cell *162*, 96–107.

Cora, E., Pandey, R.R., Xiol, J., Taylor, J., Sachidanandam, R., McCarthy, A.A., and Pillai, R.S. (2014). The MID-PIWI module of Piwi proteins specifies nucleotide- and strand-biases of piRNAs. RNA *20*, 773–781.

Cowtan, K. (2006). The Buccaneer software for automated model building. 1. Tracing protein chains. Acta Crystallogr. D Biol. Crystallogr. *62*, 1002–1011.

Czech, B., and Hannon, G.J. (2011). Small RNA sorting: matchmaking for Argonautes. Nat. Rev. Genet. *12*, 19–31.

Czech, B., and Hannon, G.J. (2016). One loop to rule them all: the ping-pong cycle and piRNA-guided silencing. Trends Biochem. Sci. *41*, 324–337.

Elkayam, E., Kuhn, C.D., Tocilj, A., Haase, A.D., Greene, E.M., Hannon, G.J., and Joshua-Tor, L. (2012). The structure of human argonaute-2 in complex with miR-20a. Cell *150*, 100–110.

Emsley, P., and Cowtan, K. (2004). Coot: model-building tools for molecular graphics. Acta Crystallogr. D Biol. Crystallogr. *60*, 2126–2132.

Evans, P.R., and Murshudov, G.N. (2013). How good are my data and what is the resolution? Acta Crystallogr. D Biol. Crystallogr. *69*, 1204–1214.

Faehnle, C.R., Elkayam, E., Haase, A.D., Hannon, G.J., and Joshua-Tor, L. (2013). The making of a slicer: activation of human Argonaute-1. Cell Rep. *3*, 1901–1909.

Feltzin, V.L., Khaladkar, M., Abe, M., Parisi, M., Hendriks, G.J., Kim, J., and Bonini, N.M. (2015). The exonuclease Nibbler regulates age-associated traits and modulates piRNA length in *Drosophila*. Aging Cell *14*, 443–452.

Frank, F., Sonenberg, N., and Nagar, B. (2010). Structural basis for 5′-nucleotide base-specific recognition of guide RNA by human AGO2. Nature *465*, 818–822.

Ghildiyal, M., and Zamore, P.D. (2009). Small silencing RNAs: an expanding universe. Nat. Rev. Genet. *10*, 94–108.

Gu, S., Jin, L., Huang, Y., Zhang, F., and Kay, M.A. (2012). Slicing-independent RISC activation requires the argonaute PAZ domain. Curr. Biol. *22*, 1536–1542.

Gunawardane, L.S., Saito, K., Nishida, K.M., Miyoshi, K., Kawamura, Y., Nagami, T., Siomi, H., and Siomi, M.C. (2007). A slicer-mediated mechanism for repeat-associated siRNA 5′ end formation in *Drosophila*. Science *315*, 1587–1590.

Han, B.W., Wang, W., Li, C., Weng, Z., and Zamore, P.D. (2015). Noncoding RNA. piRNA-guided transposon cleavage initiates Zucchini-dependent, phased piRNA production. Science *348*, 817–821.

Homolka, D., Pandey, R.R., Goriaux, C., Brasset, E., Vaury, C., Sachidanandam, R., Fauvarque, M.O., and Pillai, R.S. (2015). PIWI slicing and RNA elements in precursors instruct directional primary piRNA biogenesis. Cell Rep. *12*, 418–428.

Horwich, M.D., Li, C., Matranga, C., Vagin, V., Farley, G., Wang, P., and Zamore, P.D. (2007). The *Drosophila* RNA methyltransferase, DmHen1, modifies germline piRNAs and single-stranded siRNAs in RISC. Curr. Biol. *17*, 1265–1272.

Ipsaro, J.J., Haase, A.D., Knott, S.R., Joshua-Tor, L., and Hannon, G.J. (2012). The structural biochemistry of Zucchini implicates it as a nuclease in piRNA biogenesis. Nature *491*, 279–283.

Iwasaki, Y.W., Siomi, M.C., and Siomi, H. (2015). PIWI-interacting RNA: its biogenesis and functions. Annu. Rev. Biochem. *84*, 405–433.

Izumi, N., Shoji, K., Sakaguchi, Y., Honda, S., Kirino, Y., Suzuki, T., Katsuma, S., and Tomari, Y. (2016). Identification and functional analysis of the pre-piRNA 3′ Trimmer in silkworms. Cell *164*, 962–973.

Jo, M.H., Shin, S., Jung, S.R., Kim, E., Song, J.J., and Hohng, S. (2015). Human Argonaute 2 has diverse reaction pathways on target RNAs. Mol. Cell *59*, 117–124.

Kawaoka, S., Hayashi, N., Suzuki, Y., Abe, H., Sugano, S., Tomari, Y., Shimada, T., and Katsuma, S. (2009). The *Bombyx* ovary-derived cell line endogenously expresses PIWI/PIWI-interacting RNA complexes. RNA *15*, 1258–1264.

Kawaoka, S., Izumi, N., Katsuma, S., and Tomari, Y. (2011). 3′ end formation of PIWI-interacting RNAs *in vitro*. Mol. Cell *43*, 1015–1022.

Kobayashi, H., and Tomari, Y. (2016). RISC assembly: Coordination between small RNAs and Argonaute proteins. Biochim. Biophys. Acta *1859*, 71–81.

Kwak, P.B., and Tomari, Y. (2012). The N domain of Argonaute drives duplex unwinding during RISC assembly. Nat. Struct. Mol. Biol. *19*, 145–151.

Lewis, B.P., Burge, C.B., and Bartel, D.P. (2005). Conserved seed pairing, often flanked by adenosines, indicates that thousands of human genes are microRNA targets. Cell *120*, 15–20.

Malone, C.D., and Hannon, G.J. (2009). Small RNAs as guardians of the genome. Cell *136*, 656–668.

Meister, G. (2013). Argonaute proteins: functional insights and emerging roles. Nat. Rev. Genet. *14*, 447–459.

Miyoshi, K., Tsukumo, H., Nagami, T., Siomi, H., and Siomi, M.C. (2005). Slicer function of *Drosophila* Argonautes and its involvement in RISC formation. Genes Dev. *19*, 2837–2848.

Mohn, F., Handler, D., and Brennecke, J. (2015). Noncoding RNA. piRNA-guided slicing specifies transcripts for Zucchini-dependent, phased piRNA biogenesis. Science *348*, 812–817.

Nakanishi, K., Weinberg, D.E., Bartel, D.P., and Patel, D.J. (2012). Structure of yeast Argonaute with guide RNA. Nature *486*, 368–374.

Nakanishi, K., Ascano, M., Gogakos, T., Ishibe-Murakami, S., Serganov, A.A., Briskin, D., Morozov, P., Tuschl, T., and Patel, D.J. (2013). Eukaryote-specific insertion elements control human ARGONAUTE slicer activity. Cell Rep. *3*, 1893–1900.

Nishida, K.M., Iwasaki, Y.W., Murota, Y., Nagao, A., Mannen, T., Kato, Y., Siomi, H., and Siomi, M.C. (2015). Respective functions of two distinct Siwi complexes assembled during PIWI-interacting RNA biogenesis in *Bombyx* germ cells. Cell Rep. *10*, 193–203.

Nishimasu, H., Ishizu, H., Saito, K., Fukuhara, S., Kamatani, M.K., Bonnefond, L., Matsumoto, N., Nishizawa, T., Nakanaga, K., Aoki, J., et al. (2012). Structure and function of Zucchini endoribonuclease in piRNA biogenesis. Nature *491*, 284–287.

Okamura, K., and Lai, E.C. (2008). Endogenous small interfering RNAs in animals. Nat. Rev. Mol. Cell Biol. *9*, 673–678.

Park, J.H., and Shin, C. (2015). Slicer-independent mechanism drives small-RNA strand separation during human RISC assembly. Nucleic Acids Res. *43*, 9418–9433.

Saito, K., Nishida, K.M., Mori, T., Kawamura, Y., Miyoshi, K., Nagami, T., Siomi, H., and Siomi, M.C. (2006). Specific association of Piwi with rasiRNAs derived from retrotransposon and heterochromatic regions in the *Drosophila* genome. Genes Dev. *20*, 2214–2222.

Saito, K., Sakaguchi, Y., Suzuki, T., Suzuki, T., Siomi, H., and Siomi, M.C. (2007). Pimet, the *Drosophila* homolog of HEN1, mediates 2′-*O*-methylation of Piwi-interacting RNAs at their 3′ ends. Genes Dev. *21*, 1603–1608.

Salomon, W.E., Jolly, S.M., Moore, M.J., Zamore, P.D., and Serebrov, V. (2015). Single-molecule imaging reveals that Argonaute reshapes the binding properties of its nucleic acid guides. Cell *162*, 84–95.

Schirle, N.T., and MacRae, I.J. (2012). The crystal structure of human Argonaute2. Science *336*, 1037–1040.

Schirle, N.T., Sheu-Gruttadauria, J., and MacRae, I.J. (2014). Structural basis for microRNA targeting. Science *346*, 608–613.

Schirle, N.T., Sheu-Gruttadauria, J., Chandradoss, S.D., Joo, C., and MacRae, I.J. (2015). Water-mediated recognition of t1-adenosine anchors Argonaute2 to microRNA targets. eLife *4*, e07646.

Schürmann, N., Trabuco, L.G., Bender, C., Russell, R.B., and Grimm, D. (2013). Molecular dissection of human Argonaute proteins by DNA shuffling. Nat. Struct. Mol. Biol. *20*, 818–826.

Sheng, G., Zhao, H., Wang, J., Rao, Y., Tian, W., Swarts, D.C., van der Oost, J., Patel, D.J., and Wang, Y. (2014). Structure-based cleavage mechanism of *Thermus thermophilus* Argonaute DNA guide strand-mediated DNA target cleavage. Proc. Natl. Acad. Sci. USA *111*, 652–657.

Simon, B., Kirkpatrick, J.P., Eckhardt, S., Reuter, M., Rocha, E.A., Andrade-Navarro, M.A., Sehr, P., Pillai, R.S., and Carlomagno, T. (2011). Recognition of 2′-*O*-methylated 3′-end of piRNA by the PAZ domain of a Piwi protein. Structure *19*, 172–180.

Siomi, H., and Siomi, M.C. (2009). On the road to reading the RNA-interference code. Nature *457*, 396–404.

Song, J.J., Smith, S.K., Hannon, G.J., and Joshua-Tor, L. (2004). Crystal structure of Argonaute and its implications for RISC slicer activity. Science *305*, 1434–1437.

Tang, W., Tu, S., Lee, H.C., Weng, Z., and Mello, C.C. (2016). The RNase PARN-1 trims piRNA 3′ ends to promote transcriptome surveillance in *C. elegans*. Cell *164*, 974–984.

Terwilliger, T.C. (2000). Maximum-likelihood density modification. Acta Crystallogr. D Biol. Crystallogr. *56*, 965–972.

Tian, Y., Simanshu, D.K., Ma, J.B., and Patel, D.J. (2011). Structural basis for piRNA 2′-*O*-methylated 3′-end recognition by Piwi PAZ (Piwi/Argonaute/Zwille) domains. Proc. Natl. Acad. Sci. USA *108*, 903–910.

Vagin, A., and Teplyakov, A. (2010). Molecular replacement with MOLREP. Acta Crystallogr. D Biol. Crystallogr. *66*, 22–25.

Wang, Y., Sheng, G., Juranek, S., Tuschl, T., and Patel, D.J. (2008a). Structure of the guide-strand-containing argonaute silencing complex. Nature *456*, 209–213.

Wang, Y., Juranek, S., Li, H., Sheng, G., Tuschl, T., and Patel, D.J. (2008b). Structure of an argonaute silencing complex with a seed-containing guide DNA and target RNA duplex. Nature *456*, 921–926.

Wang, Y., Juranek, S., Li, H., Sheng, G., Wardle, G.S., Tuschl, T., and Patel, D.J. (2009). Nucleation, propagation and cleavage of target RNAs in Ago silencing complexes. Nature *461*, 754–761.

Wang, W., Yoshikawa, M., Han, B.W., Izumi, N., Tomari, Y., Weng, Z., and Zamore, P.D. (2014). The initial uridine of primary piRNAs does not create the tenth adenine that Is the hallmark of secondary piRNAs. Mol. Cell *56*, 708–716.

Wang, H., Ma, Z., Niu, K., Xiao, Y., Wu, X., Pan, C., Zhao, Y., Wang, K., Zhang, Y., and Liu, N. (2016). Antagonistic roles of Nibbler and Hen1 in modulating piRNA 3′ ends in *Drosophila*. Development *143*, 530–539.

Waterman, D.G., Winter, G., Parkhurst, J.M., Fuentes-Montero, L., Hattne, J., Brewster, A., Sauter, N.K., Evans, G., and Rosenstrom, P. (2013). The DIALS framework for integration software. CCP4 Newsletter *49*, 16–19.

Weick, E.M., and Miska, E.A. (2014). piRNAs: from biogenesis to function. Development *141*, 3458–3471.

Xiol, J., Spinelli, P., Laussmann, M.A., Homolka, D., Yang, Z., Cora, E., Couté, Y., Conn, S., Kadlec, J., Sachidanandam, R., et al. (2014). RNA clamping by Vasa assembles a piRNA amplifier complex on transposon transcripts. Cell *157*, 1698–1711.

Yao, C., Sasaki, H.M., Ueda, T., Tomari, Y., and Tadakuma, H. (2015). Single-molecule analysis of the target cleavage reaction by the *Drosophila* RNAi enzyme complex. Mol. Cell *59*, 125–132.

Yuan, Y.R., Pei, Y., Ma, J.B., Kuryavyi, V., Zhadina, M., Meister, G., Chen, H.Y., Dauter, Z., Tuschl, T., and Patel, D.J. (2005). Crystal structure of *A. aeolicus* argonaute, a site-specific DNA-guided endoribonuclease, provides insights into RISC-mediated mRNA cleavage. Mol. Cell *19*, 405–419.

Zeng, L., Zhang, Q., Yan, K., and Zhou, M.M. (2011). Structural insights into piRNA recognition by the human PIWI-like 1 PAZ domain. Proteins *79*, 2004–2009.

STAR★METHODS

KEY RESOURCES TABLE

REAGENT or RESOURCE	SOURCE	IDENTIFIER
Antibodies		
Mouse monoclonal anti-Siwi antibody	Nishida et al., 2015	N/A
Dynabeads Protein G	Invitrogen	Cat# 10009D
Chemicals, Peptides, and Recombinant Proteins		
CNBr-activated Sepharose 4 Fast Flow	GE Healthcare	Cat# 17098101
Thermolysin	Promega	Cat# V4001
Critical Commercial Assays		
T7 High Yield Transcription Kit	Epicenter	Cat# AS3107
Deposited Data		
Atomic coordinates, Siwi-piRISC	This paper	PDB: 5GUH
Experimental Models: Cell Lines		
BmN4 cells	Kawaoka et al., 2009	N/A
Recombinant DNA		
pIB-3 × FLAG-Siwi	Nishida et al., 2015	N/A
pIB-3 × FLAG-Siwi, various mutants	This paper	N/A
Sequence-Based Reagents		
Primer sequences	Table S2	N/A
Software and Algorithms		
DIALS	Waterman et al., 2013	http://dials.lbl.gov
AIMLESS	Evans and Murshudov, 2013	http://www.ccp4.ac.uk/html/aimless.html
MOLREP	Vagin and Teplyakov, 2010	http://www.ccp4.ac.uk/html/molrep.html
Buccaneer	Cowtan, 2006	http://www.ysbl.york.ac.uk/~cowtan/buccaneer/buccaneer.html
COOT	Emsley and Cowtan, 2004	http://www2.mrc-lmb.cam.ac.uk/personal/pemsley/coot
PHENIX	Adams et al., 2010	https://www.phenix-online.org
RESOLVE	Terwilliger, 2000	https://solve.lanl.gov/Resolve/resolve.html
CueMol	N/A	http://www.cuemol.org
Other		
EX-CELL 420 Medium	Sigma-Aldrich	Cat# 14420C
FuGENE HD	Promega	Cat# E2311

(-

CONTACT FOR REAGENT AND RESOURCE SHARING

Further information and requests for reagents may be directed to, and will be fulfilled by the corresponding author Osamu Nureki (nureki@bs.s.u-tokyo.ac.jp).

EXPERIMENTAL MODEL AND SUBJECT DETAILS

Cell Lines

BmN4 cells were cultured at 27°C in EX-CELL 420 medium (Sigma-Aldrich), supplemented with 10% fetal bovine serum (Equitech-Bio) and Penicillin-Streptomycin-Glutamine (Thermo Fisher).

METHOD DETAILS

Purification of the Siwi-piRISC

The anti-Siwi monoclonal antibody (30 mg) (Nishida et al., 2015) was coupled with CNBr-activated Sepharose 4 Fast Flow beads (12 ml) (GE Healthcare), according to the manufacturer's instructions. BmN4 cells (~9 × 10^8 cells) were suspended in buffer

30 mM Tris-HCl [pH 7.3], 300 mM NaCl, 1 mM EDTA, 0.1% NP-40, 1 mM DTT, 10% glycerol, 5 μg/ml aprotinin, 2 μg/ml leupeptin and 1 μg/ml pepstatin), lysed by a homogenizer, and then centrifuged. The supernatant was incubated with the anti-Siwi antibody-conjugated beads at 4°C for 4 hr, and the mixture was then loaded into an Econo-Column (Bio-Rad). The beads were washed three times with buffer (50 mM Tris-HCl [pH 8.0], 300 mM NaCl, 0.5 mM $CaCl_2$, 0.1% NP-40, 1 mM DTT and 10% glycerol), and then incubated with thermolysin (2 mg) (Promega) at 4°C for 12 hr, to release the Siwi-piRISC core. The Siwi-piRISC core was loaded onto a HiTrap Heparin HP column (GE Healthcare), equilibrated with buffer (50 mM Tris-HCl [pH 8.0], 200 mM NaCl, 1 mM DTT and 10% glycerol), and it was then eluted using a linear gradient of 0.2–2 M NaCl. The Siwi-piRISC core was further purified by chromatography on a HiLoad 16/600 Superdex 200 column (GE Healthcare), equilibrated with buffer (10 mM Tris-HCl [pH 8.0], 300 mM NaCl, 1 mM DTT and 10% glycerol).

Crystallization and Structural Determination

The purified Siwi-piRISC was crystallized at 20°C, using the sitting-drop vapor diffusion method. The crystallization drops were formed by mixing 0.1 μl of Siwi-piRISC solution ($A_{280\ nm}$ = 10–15) and 0.1 μl of reservoir solution (50 mM potassium phosphate monobasic and 20% PEG 8000). The crystals were cryoprotected by the reservoir solution supplemented with 20% glycerol. X-ray diffraction data were collected at 100 K on the beamline BL41XU at SPring-8 (Hyogo, Japan). The diffraction data were processed using DIALS (Waterman et al., 2013) and AIMLESS (Evans and Murshudov, 2013). The initial phases were calculated by molecular replacement with MOLREP (Vagin and Teplyakov, 2010), using the hAgo2 structure (PDB: 4OLA) (Schirle and MacRae, 2012) as the search model. The initial model was automatically built using Buccaneer (Cowtan, 2006), and then improved by manual model building using COOT (Emsley and Cowtan, 2004) and structural refinement with PHENIX (Adams et al., 2010), resulting in a clear electron density for the MID and PIWI domains. Subsequently, molecular replacement was performed with MOLREP, using the structure of the isolated PAZ domain from the Hiwi1 structure (PDB: 3O7V) (Tian et al., 2011) as the search model. The electron density map was improved by density modification with RESOLVE (Terwilliger, 2000), and the model was iteratively built and refined using COOT and PHENIX, respectively. The data collection and refinement statistics are summarized in Table S1. All molecular graphics were prepared with CueMol (http://www.cuemol.org).

Small RNA Isolation from the Immunopurified Siwi Complex

Immunoprecipitation was performed essentially as described previously (Saito et al., 2006). BmN4 lysates were prepared in binding buffer (30 mM HEPES [pH 7.4], 150 mM potassium acetate, 5 mM magnesium acetate, 5 mM DTT, 0.1% Tergitol-type NP-40, 5 μg/ml aprotinin, 2 μg/ml leupeptin and 2 μg/ml pepstatin), and then incubated with an anti-Siwi antibody bound to Dynabeads Protein G (Invitrogen) in the presence of 500 mM NaCl. The beads were then washed three times with binding buffer supplemented with 500 mM NaCl, and twice with binding buffer. Total RNAs were eluted from the beads by phenol-chloroform treatment, and then precipitated with ethanol. The RNAs were dephosphorylated with Antarctic Phosphatase (NEB) and radiolabeled with ^{32}P-γ-ATP using T4 PNK (NEB).

Plasmid Construction

The expression vector for FLAG-tagged Siwi was generated by Gateway Technology (Invitrogen), using the pIB-3 × FLAG vector. The expression vectors for the FLAG-Siwi mutants were generated by inverse PCR, using the wild-type FLAG-Siwi vector as the template. The sequences of the DNA oligos used for inverse PCR are listed in Table S2.

In Vitro Target RNA Cleavage Assay

Cleavage assays were performed as described previously (Miyoshi et al., 2005). The sequence of the RNA substrate used is 5′-GGGAGUCCAGAUUUGAAUCCGUUAGAUUACAAUCAAGCUUAUCGAUACCGUCGACCUCGAGGGG-3′ (64 nt), which corresponds to part of the *Bmmar6* transposon mRNA. The RNA substrate was prepared by in vitro transcription using a DNA template, which was amplified by PCR using the two DNA oligos, Target-F and Target-R (Table S2). In vitro transcription was performed with a T7 High Yield Transcription Kit (Epicenter) in the presence of ^{32}P-α-UTP.

QUANTIFICATION AND STATISTICAL ANALYSIS

RNA cleavage and piRNA loading experiments were repeated three times, and representative results were shown.

DATA AND SOFTWARE AVAILABILITY

Data Resources

The atomic coordinates of the Siwi-piRISC have been deposited in the Protein Data Bank: 5GUH.

Cell

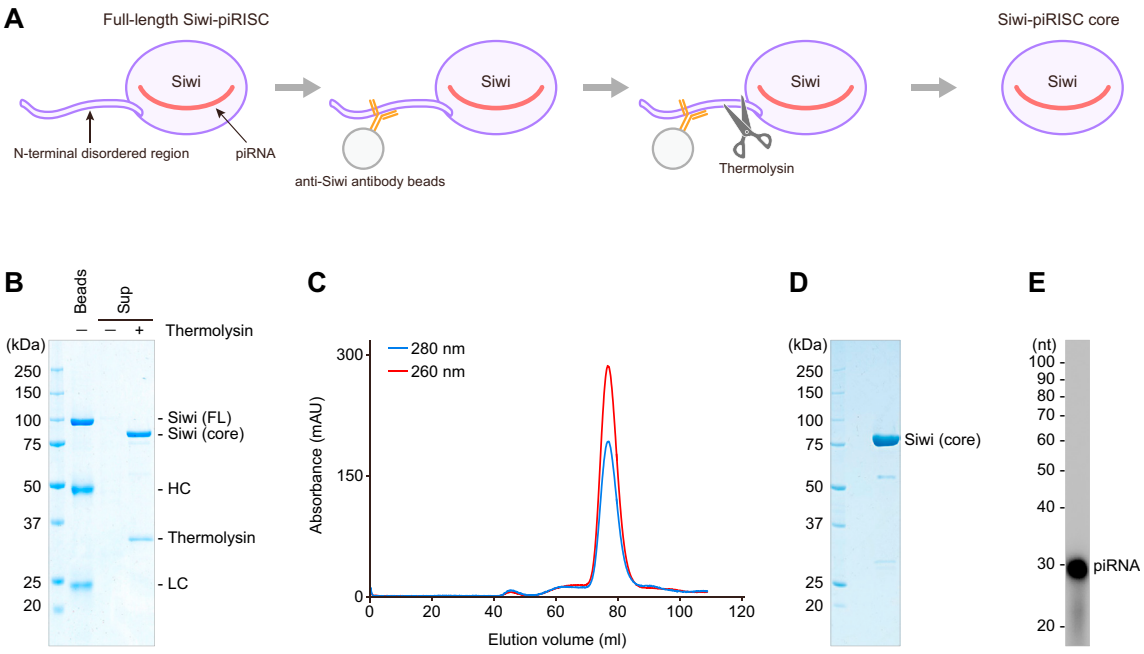

Figure S1. Preparation of the Siwi-piRISC, Related to Figure 1

(A) Purification scheme of the endogenous Siwi-piRISC from BmN4 cells.

(B) Separation of the Siwi-piRISC core from the anti-Siwi antibody beads. The full-length (FL) Siwi-piRISC bound to the antibody beads was incubated in the absence and presence of thermolysin at 4°C overnight. The untreated beads and the supernatants were then analyzed by SDS-PAGE. The gel was stained with SimplyBlue SafeStain (Invitrogen). HC, heavy chain; LC, light chain.

(C) Elution profile of the purified Siwi-piRISC core from the HiLoad 16/600 Superdex 200 column.

(D) SDS-PAGE analysis of the purified Siwi-piRISC core. The gel was stained with SimplyBlue SafeStain.

(E) Denaturing urea-PAGE analysis of the purified Siwi-piRISC core. The bound piRNA was 5′ ^{32}P-end labeled.

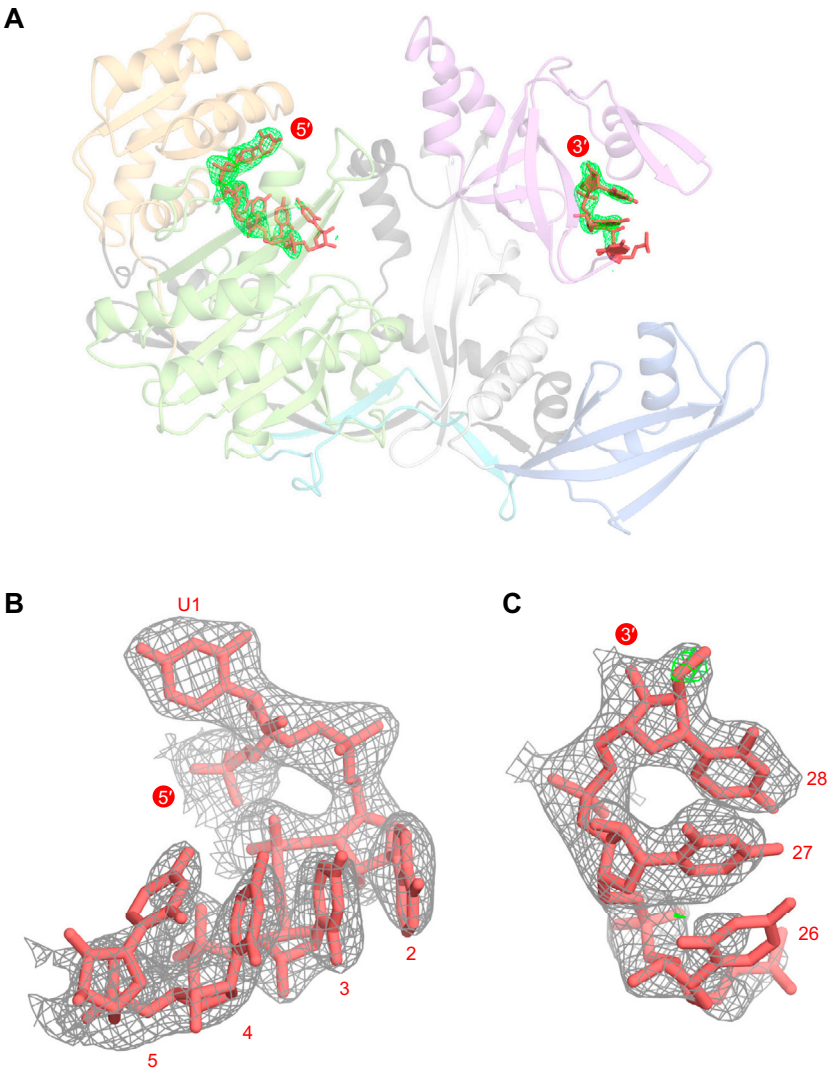

Figure S2. Electron Density Map, Related to Figure 1

(A) $mF_O - DF_C$ omit electron density map for the bound piRNA (green mesh, contoured at 3.5σ).
(B) $2mF_O - DF_C$ electron density map for the piRNA 5′ segment (gray mesh, contoured at 1σ).
(C) $2mF_O - DF_C$ electron density map for the piRNA 3′ segment (gray mesh, contoured at 1σ).
The $mF_O - DF_C$ omit electron density map for the 2′-*O*-methyl group is depicted as a green mesh (contoured at 2.2σ).

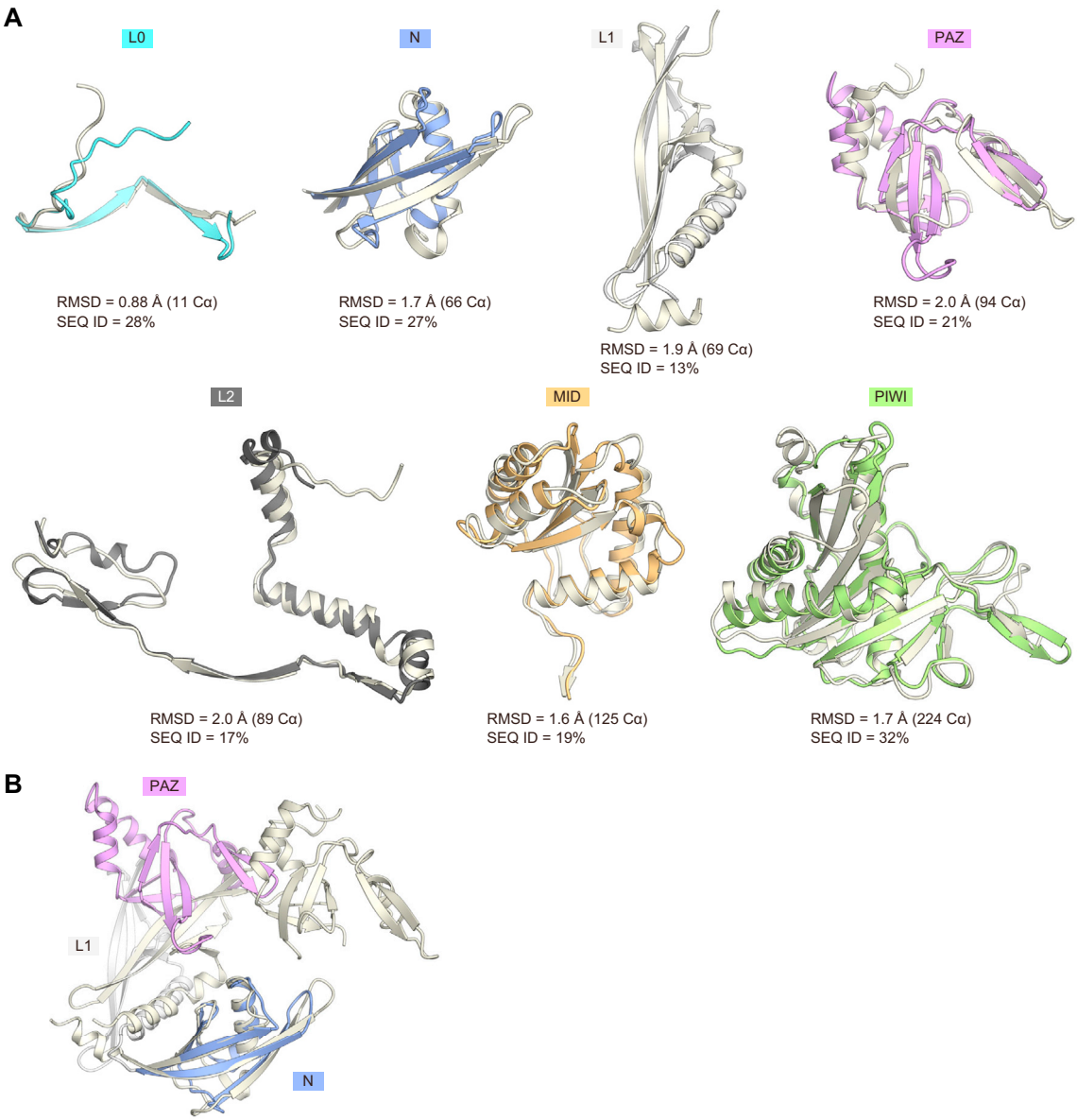

Figure S3. Structural Comparison between the Individual Domains of Siwi and hAgo2, Related to Figure 2

(A) Superimpositions of the individual domains of Siwi (colored) and hAgo2 (PDB: 4W5N) (beige). Sequence identities and root mean square deviation (RMSD) values for equivalent Cα atoms are shown below the structures.

(B) Superimpositions of the N-PAZ lobe of Siwi (colored) and hAgo2 (PDB: 4W5N) (beige), based on their N domains.

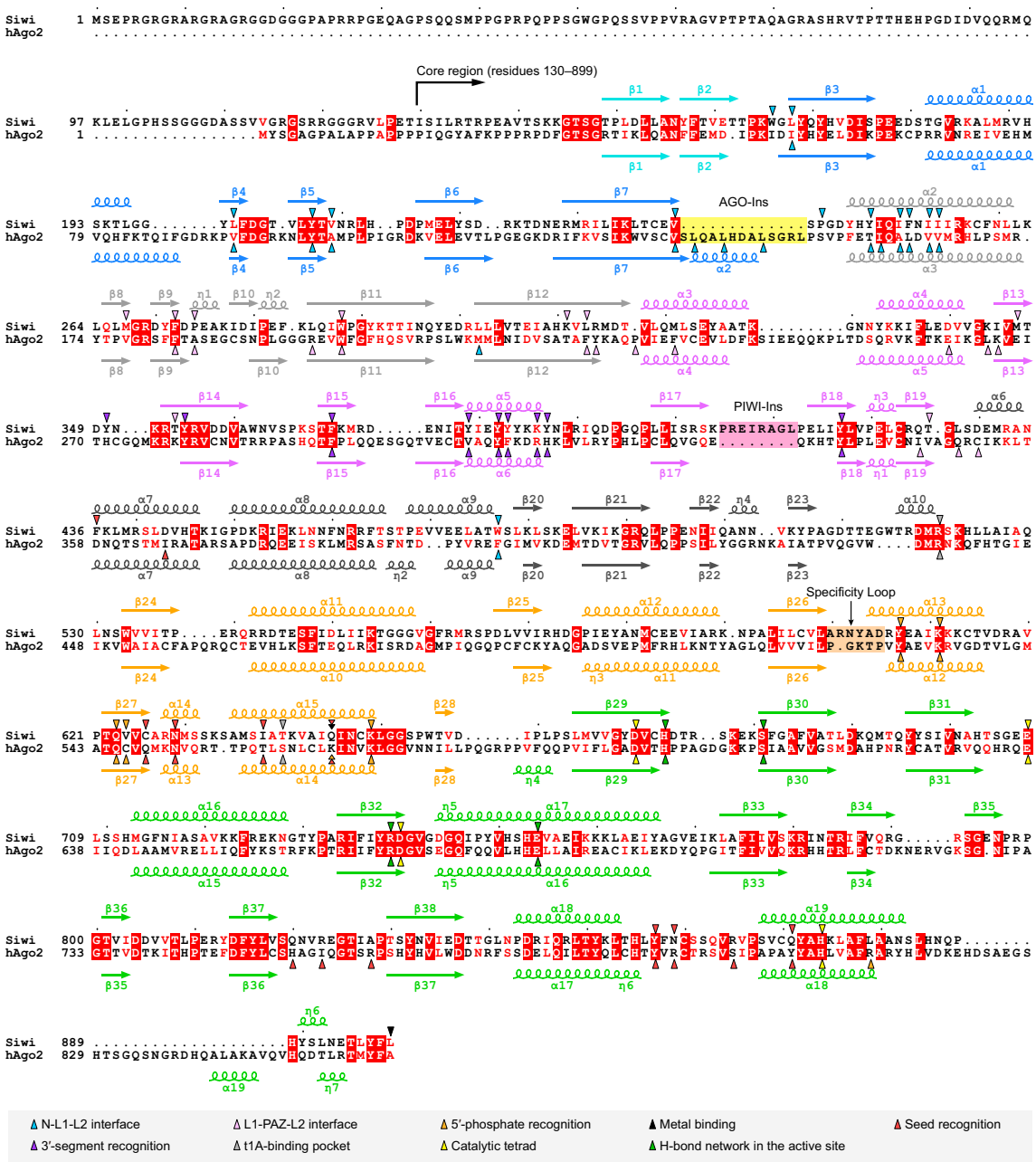

Figure S4. Structure-Guided Sequence Alignment of Siwi and of hAgo2, Related to Figure 2

The structures of Siwi and hAgo2 (PDB: 4W5N) were superimposed by the secondary-structure matching (SSM) algorithm, using CueMol (http://www.cuemol.org), and then the sequence alignment was manually refined. The AGO- and PIWI-specific insertions are highlighted in yellow and magenta, respectively. The specificity loop is highlighted in orange. Key residues are marked by triangles.

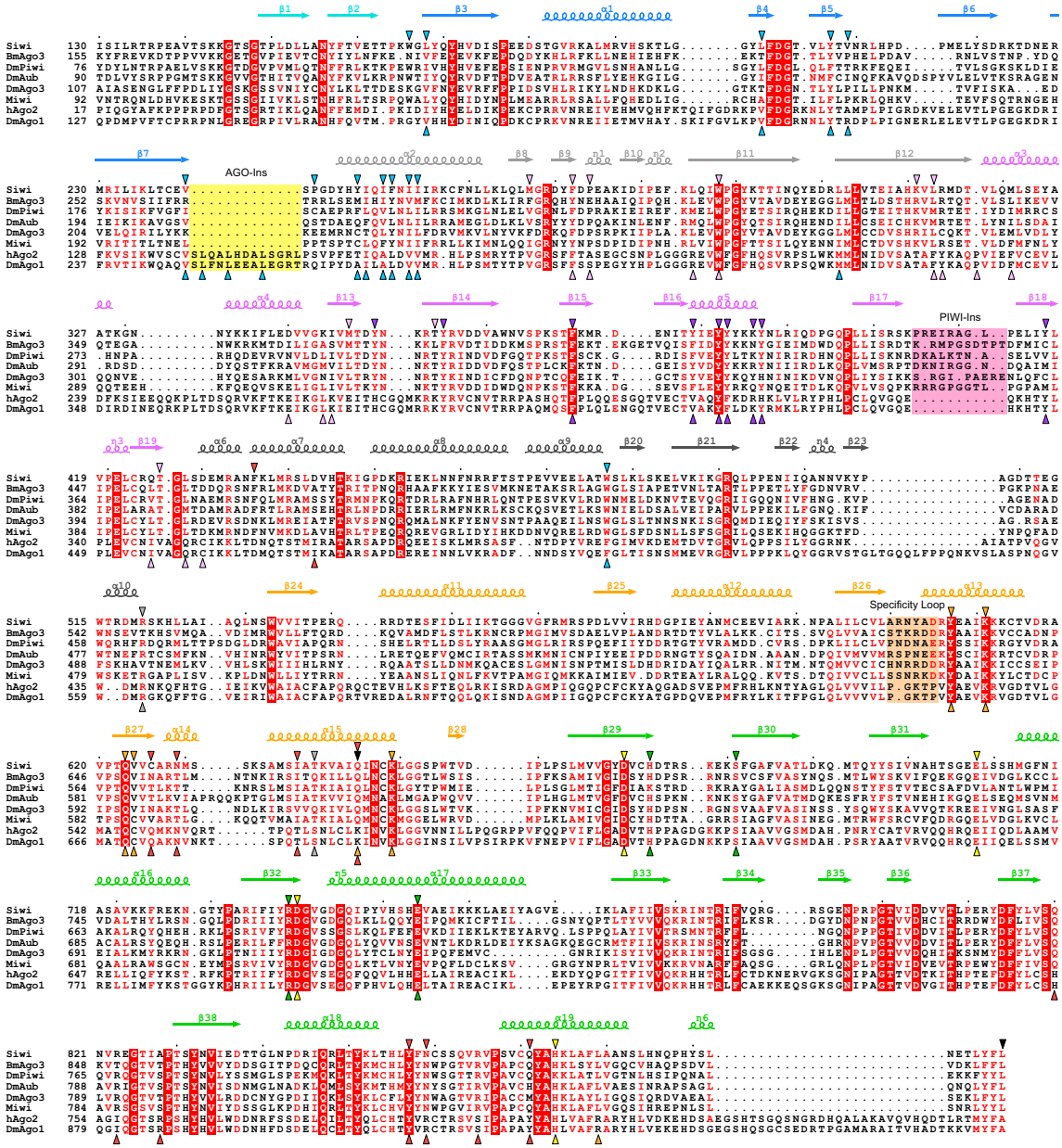

Figure S5. Multiple Sequence Alignment of the Argonaute Proteins, Related to Figure 2

The secondary structure of Siwi is indicated above the sequences. Key residues are marked by triangles. The figure was prepared using Clustal Omega (http://www.ebi.ac.uk/Tools/msa/clustalo) and ESPript3 (http://espript.ibcp.fr/ESPript/ESPript).

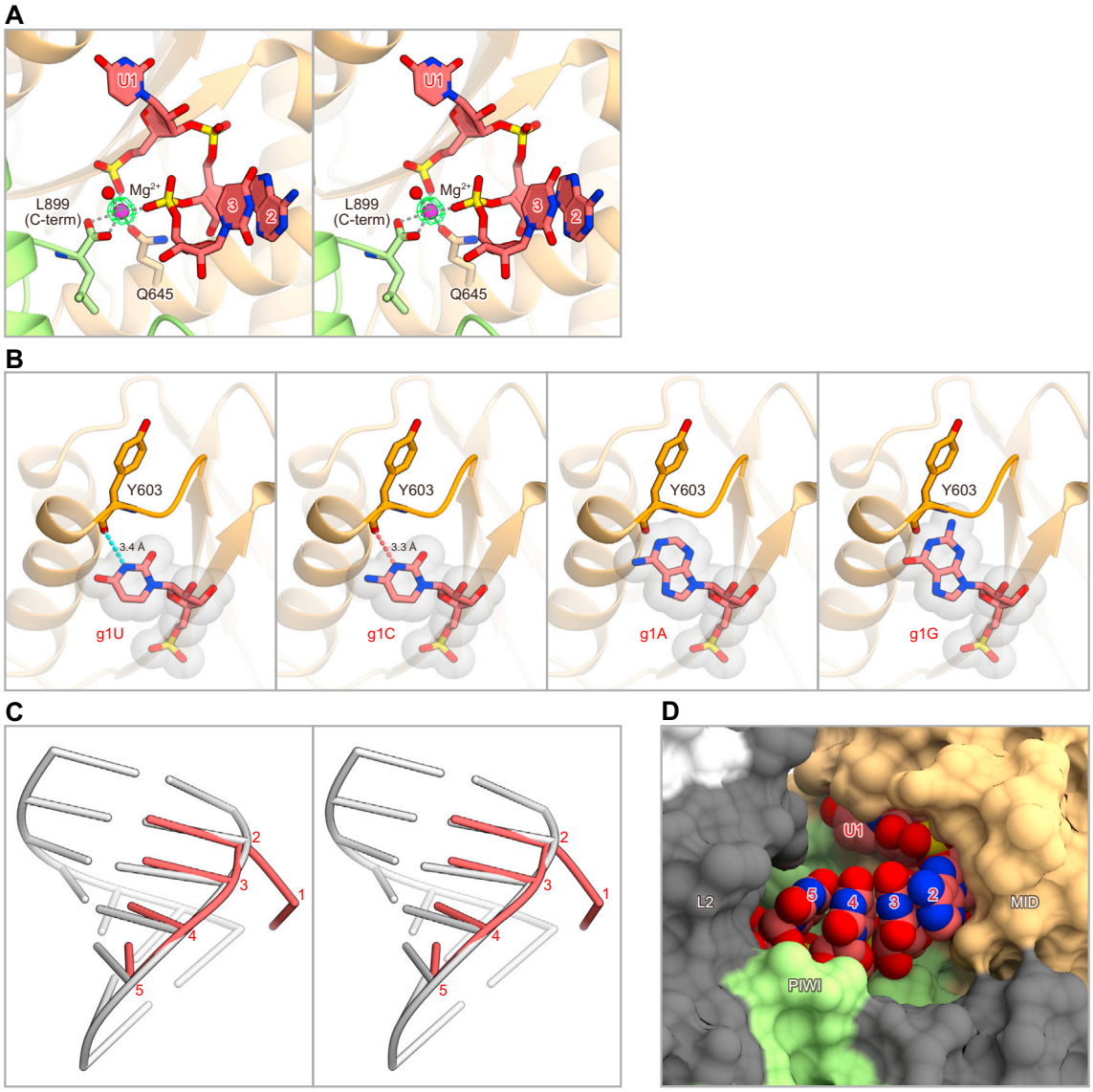

Figure S6. Recognition of the Guide 5′ Segment, Related to Figure 3

(A) $mF_O - DF_C$ omit electron density map for the bound Mg^{2+} ion (green mesh, contoured at 10σ).

(B) g1U recognition by Siwi. The specificity loop in the MID domain is highlighted in orange. The modeled A, G and C at the g1 position would form steric clashes or repulsion with Tyr603 in the specificity loop. The favorable and unfavorable interactions are indicated by cyan and red dashed lines, respectively.

(C) Superimposition of the 5′ segment of the Siwi-bound piRNA (red) onto an A-form RNA duplex (gray) (stereoview).

(D) Binding of the piRNA seed region to the Siwi MID-PIWI lobe.

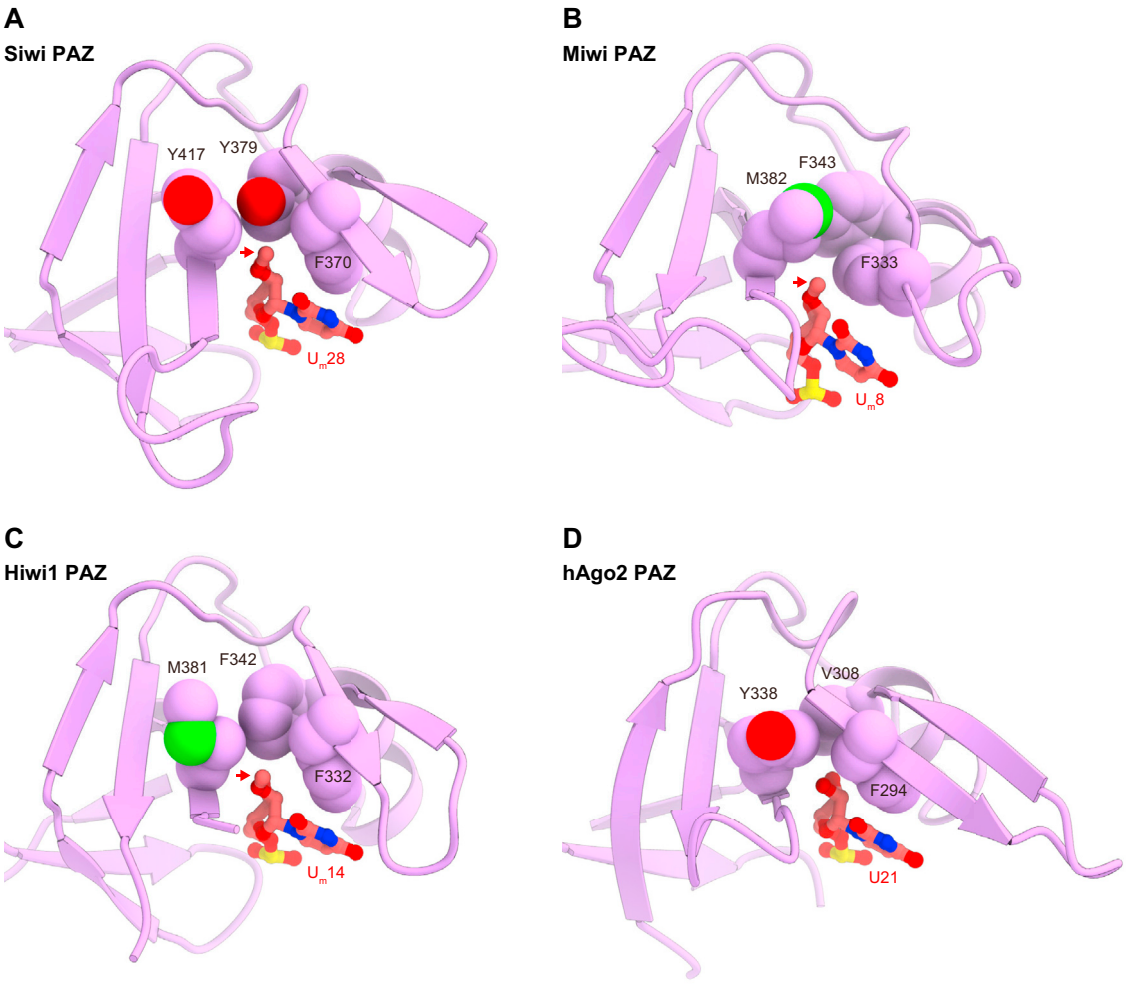

Figure S7. Recognition of the Guide 3′ Segment, Related to Figure 4

(A–D) PAZ domains of Siwi (A), Miwi (PDB: 2XFM) (B), Hiwi1 (PDB: 3O7V) (C), and hAgo2 (PDB: 4W5N) (D). The 2′-*O*-methyl group is indicated by red arrows.